

## Do plasmoids induce fast magnetic reconnection in well-resolved current sheets in 2D MHD simulations?

GIOVANI H. VICENTIN ,<sup>1</sup> GRZEGORZ KOWAL ,<sup>2</sup> ELISABETE M. DE GOUVEIA DAL PINO ,<sup>1</sup> AND ALEX LAZARIAN ,<sup>3</sup>

<sup>1</sup>Departamento de Astronomia, Universidade de São Paulo, Rua do Matão 1226, 05508-090, São Paulo, Brazil

<sup>2</sup>Escola de Artes, Ciências e Humanidades, Universidade de São Paulo, Rua Arlindo Bettio 1000, 03828-000, São Paulo, Brazil

<sup>3</sup>Department of Astronomy, University of Wisconsin, 475 North Charter Street, Madison, Wisconsin 53706, USA

Submitted to ApJ

### ABSTRACT

We investigate the development of tearing-mode instability using the highest resolution two-dimensional magnetohydrodynamic simulations of reconnecting current sheets on a uniform grid, for Lundquist numbers  $10^3 \leq S \leq 2 \times 10^5$ . Although the tearing-mode instability is commonly thought to trigger a plasmoid cascade that enables fast reconnection—i.e., independent of  $S$ —our results, in broad agreement with the recent findings of Morillo & Alexakis (2025), challenge this belief. We demonstrate a Sweet-Parker scaling of the reconnection rate  $V_{\text{rec}} \sim S^{-1/2}$  up to Lundquist numbers  $S \sim 10^4$ . For larger values, plasmoid formation sets in leading to a slight enhancement of the reconnection rate,  $V_{\text{rec}} \sim S^{-1/3}$ , consistent with the prediction from linear tearing mode induced reconnection, indicating that reconnection remains resistivity dependent, and therefore slow. In our simulations, the plasmoids do not form a cascade of mergers, as they are rapidly advected out of the reconnection layer. Our findings call for the revision of the role of plasmoid formation in 2D high Lundquist number magnetic reconnection. Even if future studies demonstrate that 2D plasmoid-reconnection becomes resistivity-independent at sufficiently large  $S$ , directly extending those results to 3D astrophysical environments is not justified, as in realistic circumstances, the increase of  $S$  also raises the Reynolds number of the outflows, making it essential to account for the dominant role of turbulence.

**Keywords:** Magnetohydrodynamics (MHD) — Magnetic Reconnection — Plasmoids — Methods: Numerical

### 1. INTRODUCTION

Magnetic reconnection is a fundamental plasma process in which magnetic field free energy associated with reversals of magnetic field components is transferred to other forms of energy. This process is frequently described in terms of magnetic field topology change, with magnetic lines breaking and reconnecting, allowing the conversion of magnetic energy into kinetic energy, heat, and particle acceleration. This mechanism has long been recognized as playing a central role not only in laboratory plasmas (Taylor 1986; Yamada et al. 1994, 1997), but also in a wide range of astrophysical environments, including solar flares (Parker 1957, 1988; Masuda et al. 1994; Priest & Forbes 2002), the Earth’s magnetosphere (Kivelson & Russell 1995), proto-stellar disks (de Gouveia Dal Pino et al. 2010a,b), and relativistic sources such as microquasars, active galactic nuclei (AGNs), and

gamma-ray-bursts (GRBs) (e.g., de Gouveia Dal Pino & Lazarian 2005; Giannios et al. 2009; de Gouveia Dal Pino et al. 2010a; Giannios 2010; Zhang & Yan 2011; Nalewajko et al. 2011; Kadovski et al. 2015, 2021; Medina-Torrezón et al. 2021; Nishikawa et al. 2021; Medina-Torrezón et al. 2023; de Gouveia Dal Pino & Medina-Torrezón 2024), pulsars (e.g., Cerutti et al. 2012), and X-ray binaries (e.g., Khiali et al. 2015).

In classical resistive magnetohydrodynamics (MHD), the Sweet–Parker model (Sweet 1958; Parker 1957) describes the reconnection that occurs in a thin, long current sheet. Although this model provides a self-consistent framework, it predicts a reconnection rate that scales as  $V_{\text{rec}}/V_A \sim S^{-1/2}$ , where  $S = LV_A/\eta$  is the Lundquist number,  $L$  is the typical length scale of the system,  $V_A$  is the Alfvén velocity, and  $\eta$  is the ohmic resistivity. In highly conducting plasmas ( $S \gg 1$ ), this

rate is far too slow to account for the fast reconnection observed in nature, mainly in astrophysical environments, where  $S \sim 10^{8-20}$ . From a physical standpoint, the sluggish nature of Sweet-Parker reconnection arises from the strong disparity of the thickness of the matter outflow  $\delta$ , set by the microscopic (resistive) scale of the Ohmic diffusion and the macroscopic (astrophysical) extent of the surface  $L$  over which reconnection takes place. Mass conservation dictates that  $V_{rec} \rightarrow 0$  as  $\delta/L \rightarrow 0$ .

To resolve this discrepancy, Petschek (1964) proposed an alternative model in which the length of the diffusion region ( $L$ ) remains of the order of its thickness ( $\delta$ ). This configuration is achieved through the presence of standing slow-mode shocks, which bend the reconnecting fluxes into an open X-point geometry, thereby enabling fast reconnection rates that depend only weakly on resistivity ( $V_{rec}/V_A \sim 1/\ln S$ ). However, Biskamp (1986) demonstrated numerically that, in resistive MHD with uniform resistivity, the Petschek X-point collapses into elongated current sheets consistent with the Sweet-Parker configuration. As a result, it became widely accepted that fast reconnection requires either non-uniform (anomalous) resistivity or additional physics beyond classical resistive MHD.

Early attempts to sustain Petschek-type reconnection invoked anomalous effects, in particular localized resistivity or two-fluid contributions such as the Hall term (e.g. Ugai 1992; Shay et al. 1999; Birn & Hesse 2001). While Hall reconnection remains a key framework in collisionless space and laboratory plasmas, numerical investigations over the following decade indicated that such mechanisms alone could not provide a universal explanation for fast reconnection in large-scale astrophysical environments, where kinetic scales are negligible compared with macroscopic system sizes. As a result, the focus of the astrophysical community shifted toward the plasmoid-mediated tearing instability as the mechanism capable of enabling fast reconnection in two-dimensional resistive MHD (Loureiro et al. 2007; Bhattacharjee et al. 2009; Uzdensky et al. 2010).<sup>1</sup>

Attempts to increase  $\delta$  appealing to instabilities have been explored in the literature. Resistive instabilities in a magnetized fluid can trigger a long-wavelength tear-

ing mode within the current sheet, driving magnetic reconnection and spawning a chain of narrow magnetic islands in a two-dimensional flow, as first demonstrated by Furth et al. (1963). Building on the notion that a continuous sheet fragments into discrete islands, Heyvaerts & Priest (1984) argued that such tearing modes might underpin the heating of the solar corona, while Lee & Fu (1985, 1986) extended the idea to Earth's magnetopause by modeling reconnection along multiple X-lines. Extensive work by S. Syrovatskii and collaborators proposed that tearing instability is a generic feature of astrophysical reconnection (see Syrovatskii 1981, and references therein).

Lazarian & Vishniac (1999), considering steady-state reconnection on the scale of the reconnection sheet  $L$ , demonstrated that the tearing instability increases  $\delta$  (see their Appendix C), yielding a reconnection rate that scales as  $S^{-3/10}$ . Although this represents an improvement over the Sweet-Parker rate, it remains far too slow to account for astrophysical reconnection.

The interest in the role of tearing instability for reconnection has been renewed more recently due to the increase in available computational power. The primary object of such studies was 2D reconnection, where higher numerical resolution is available. In this paper, we follow the trend, even though the physics of reconnection can be different in 2D and 3D.

2D numerical simulations revealed the transition from the Sweet-Parker reconnection to a regime where tearing mode instability becomes significant. In particular, it was observed that when the current sheet is sufficiently thin, the tearing instability develops. A new effect, absent in earlier theoretical models, was observed in the numerical simulations, namely, the formation of chains of magnetic islands within the 2D current sheet (Loureiro et al. 2007). These islands, commonly referred to as plasmoids, were observed to interact, merge, and grow into so-called “monster” plasmoids (Uzdensky et al. 2010; Loureiro et al. 2012), which are subsequently advected away by the 2D outflow. This 2D cascade of growing plasmoids was assumed to bring to life what earlier tearing mode theoretical studies could not accomplish, namely, the combination of tearing reconnection at the smallest resistive scales with the efficient outflow of matter from the reconnection region on the scale of the “monster” plasmoids. The size of these structures determines the thickness of the outflow and may not depend on resistivity, potentially enabling  $S$ -independent reconnection.

The subsequent studies with dedicated 2D MHD simulations (Bhattacharjee et al. 2009; Huang & Bhattacharjee 2010; Loureiro et al. 2012) reported that for high

<sup>1</sup> We do not address here the theory of 3D turbulent reconnection, where the current sheet thickness  $\delta$  is set by magnetic-field line wandering in the turbulent flow and can be comparable with  $L$  (Lazarian & Vishniac 1999). The predictions of this theory have been successfully confirmed numerically (Kowal et al. 2009, 2012; Vicentin et al. 2025) and applied to explain a broad range of space-physics and astrophysical observations (see, e.g. Lazarian et al. 2020, for a review).

Lundquist numbers, of  $S \gtrsim 10^4$ , plasmoids can induce reconnection independent of Ohmic resistivity  $\eta$ , at a universal rate of  $V_{\text{rec}} \sim 0.01 V_A$ , which is the expected Sweet-Parker rate for the critical Lundquist number of  $S_c = 10^4$ .

Applying proper boundary conditions is nontrivial in reconnection simulations. To overcome this difficulty, Bhattacharjee et al. (2009) adopted two coalescing magnetic flux tubes (Uzdensky & Kulsrud 2000) for the reconnection setup. The authors reported that in their simulations, plasmoids are formed when Lundquist numbers reach a critical value of  $S \gtrsim 3 \times 10^4 = S_c$ . In Huang & Bhattacharjee (2010), the authors repeated the 2D simulations with higher resolution and different noise amplitudes ( $\epsilon$ ), and observed that the critical Lundquist number can reach up to  $S_c = 10^5$  for  $\epsilon = 10^{-5}$ . Expanding this analysis, Huang et al. (2017) calculated the critical Lundquist number as a function of the initial noise, and found that  $S_c = 10^6$  for  $\epsilon = 10^{-30}$  (see their Fig. 10).

More recently, Morillo & Alexakis (2025) conducted high-resolution 2D MHD simulations of the Orszag & Tang (1979) vortex with an uniform-grid to investigate magnetic reconnection processes and the development of tearing mode instability. They found that when the current layer is well-resolved, specifically when the ratio between the thickness of the current sheet ( $\delta$ ) and the simulation's cell size ( $h$ ) satisfies  $\delta/h \geq 10$ , plasmoid formation is suppressed. Morillo & Alexakis (2025) observed that, under these well-resolved conditions, the reconnection rate adheres to the Sweet-Parker model, indicating a slow Lundquist number-dependent reconnection. Their simulations demonstrated that even at a Lundquist number as high as  $5 \times 10^5$ , achieved with a resolution of  $32,768^2$  grid points, no plasmoid instability developed.

The work by Morillo & Alexakis (2025) clearly demonstrated the importance of resolving the details of the current sheet for studies of tearing reconnection. However, the tearing mode instability is a genuine physical process observed both in nature and in laboratory plasma experiments (e.g., Jara-Almonte et al. 2016). This makes it essential to explore the development of the instability, keeping the resolution of the current sheet high.

To understand the nature of high Lundquist number 2D reconnection, we perform simulations that satisfy the Morillo & Alexakis (2025) criterion,  $\delta/h > 10$ , but we add a small level of noise to ensure that the instability develops, avoiding the possibility that it is suppressed by an insufficient initial perturbation.

In Section 2, we present a review of the linear theory of the tearing mode instability, which provides the the-

oretical foundation for our study. Section 3 describes the numerical setup of the simulations and the computational methods implemented. In Section 4, we present the procedure used to measure the reconnection rate in our 2D MHD simulations. Section 5 contains the main results, with particular emphasis on convergence analysis between different numerical resolutions, as well as the introduction of a new method to quantify numerical errors directly from the simulations. In Section 6, we summarize and discuss the implications of our findings and in Section 7, we present the main conclusions of the paper.

## 2. TEARING MODE INSTABILITY AND THE CRITICAL LUNDQUIST NUMBER

### 2.1. Linear Growth of the Tearing Instability

The tearing instability of thin current sheets has been the subject of detailed analysis since the seminal works of Furth et al. (1963) and Coppi et al. (1976). It arises when a magnetic configuration with antiparallel field lines develops a thin resistive layer that permits magnetic reconnection, causing exponential growth of perturbations on top of the equilibrium sheet. The character of the instability depends on how magnetic flux is redistributed across the inner resistive layer, and two asymptotic regimes can be distinguished depending on the parameter  $kaS_a^{1/4}$ , where  $a$  is the sheet half-thickness,  $k$  the perturbation wavenumber along the sheet, and  $S_a = V_A a / \eta$  the Lundquist number defined with respect to  $a$ . Here  $V_A$  is the upstream Alfvén speed and  $\eta$  the magnetic diffusivity.

When  $kaS_a^{1/4} \gg 1$  (known as *constant- $\psi$*  regime), the magnetic flux function can be regarded as constant across the inner resistive layer. In this case, the growth rate of the instability scales as

$$\gamma_{\text{FKR}} \sim \frac{V_A}{a} S_a^{-3/5} (ka)^{2/5}, \quad (1)$$

the classical result of Furth et al. (1963, hereafter FKR63). Physically, this regime corresponds to relatively short-wavelength modes, where the outer region responds rigidly. As a result, flux is reconnected slowly and the instability growth is strongly damped by resistivity.

When instead,  $kaS_a^{1/4} \ll 1$ , the flux function is no longer constant across the inner layer. In this regime (known as *non-constant- $\psi$*  regime), perturbations can redistribute magnetic flux more effectively, leading to a faster growth rate

$$\gamma_{\text{Coppi}} \sim \frac{V_A}{a} S_a^{-1/3} (ka)^{2/3}, \quad (2)$$

as obtained by [Coppi et al. \(1976\)](#). This regime applies at longer wavelengths, where the sheet is more easily destabilized because magnetic tension is weaker over larger scales.

The transition between these two regimes is set by the condition  $\Delta'\delta_{\text{in}} \sim 1$ , where  $\Delta'$  is the tearing stability parameter from outer-region matching, and  $\delta_{\text{in}}$  is the resistive inner layer width. For a Harris-type sheet, this condition yields the crossover scale

$$k_* a \sim S_a^{-1/4}. \quad (3)$$

At this wavenumber the instability achieves its maximum linear growth rate,

$$\gamma_{\text{max}} \approx C_\gamma \frac{V_A}{a} S_a^{-1/2}, \quad (4)$$

with corresponding wavenumber

$$k_{\text{max}} \approx \frac{C_k}{a S_a^{1/4}}. \quad (5)$$

The coefficients  $C_\gamma$  and  $C_k$  are of order unity but depend somewhat on the equilibrium profile and boundary conditions. Our numerical analysis for  $Pr_m = 1$  gives  $C_\gamma \approx 0.5$  and  $C_k \approx 1.05$  (see Appendix A), which are consistent with earlier work (e.g. [Loureiro et al. 2007](#); [Tenerani et al. 2015](#)).

Viscous and compressible effects further enrich this picture. Early work by [Porcelli \(1987\)](#) showed that viscosity can significantly alter growth rates and inner-layer scalings when the magnetic Prandtl number  $Pr_m = \nu/\eta$  is large. Subsequent studies, such as [Tenerani et al. \(2015\)](#), developed a systematic treatment of the visco-resistive tearing instability in Harris-type current sheets. For the case of  $P_m = 1$  considered here, however, viscosity modifies only the numerical prefactors, leaving the classical scaling laws essentially unchanged.

From a physical perspective, the key point is that thin current sheets are generically unstable. For a fixed sheet half-thickness  $a$ , the maximum tearing growth rate scales as  $\gamma_{\text{max}} \propto S_a^{-1/2}$ , i.e. it decreases with the local Lundquist number  $S_a$ . However, in a Sweet–Parker sheet the thickness itself shrinks with the global Lundquist number as  $a \sim LS^{-1/2}$ , so that the effective local parameter scales as  $S_a \sim S^{1/2}$ . Substituting this relation into the expression for  $\gamma_{\text{max}}$  yields the well-known result  $\gamma_{\text{max}}\tau_A \propto S^{1/4}$  ([Loureiro et al. 2007](#)), meaning that in practice the instability becomes stronger as  $S$  increases. Thus, beyond a critical global Lundquist number, any sufficiently long sheet will inevitably fragment into multiple plasmoids, and the linear tearing modes become the seeds for nonlinear reconnection.

In our numerical simulations we employ two complementary strategies to excite these tearing modes. First, we apply a small-amplitude random noise perturbation to the velocity field. This approach excites a broad spectrum of wavenumbers, allowing the system to select and amplify the fastest-growing tearing harmonics predicted by linear theory. Second, we impose multimode perturbations directly in Fourier space, deliberately choosing wavenumbers around  $k_{\text{max}}$  from Eq. (5). In this case, the seeded modes are those expected to grow most rapidly according to theory, ensuring that the instability develops efficiently and shortening the linear stage. These perturbation strategies therefore provide both a generic and a targeted way to trigger tearing, directly reflecting the analytical estimates of unstable modes.

## 2.2. Reconnection Rate from the Maximum-Growth Tearing Mode

[Lazarian & Vishniac \(1999\)](#) estimated the global reconnection rate by equating the tearing growth rate to the shear outflow rate. In their Appendix C, they employed the **FKR63** growth rate (Eq. 1), obtaining

$$V_{\text{rec}} \propto V_A S^{-3/10}, \quad (6)$$

with  $S \equiv V_A L/\eta$ . If instead the fastest growing tearing mode at the FKR–Coppi crossover is considered, then the maximum growth rate from Eq. (4) applies. Importantly, the growth rate  $\gamma_{\text{max}}$  increases as the sheet half-thickness  $a$  decreases. However, as argued by [Lazarian & Vishniac \(1999\)](#), a steady-state reconnection layer requires that mass outflow from the current sheet proceed at a speed limited by  $V_A$ .

This constraint implies that the inflow speed (and hence the reconnection rate) cannot grow arbitrarily as  $a$  shrinks. Rather, mass conservation requires the reconnection rate to scale with the ratio  $a/\lambda_{\parallel}$ , where  $\lambda_{\parallel}$  denotes the parallel scale of plasma exhaust along the sheet. In other words, reconnection becomes faster with larger  $a$ , while the resistive reduction of  $a$  is balanced by the need to sustain an Alfvénic outflow. This situation is directly analogous to the Sweet–Parker case, where reducing  $a$  increases resistive efficiency but is constrained by mass conservation through the global outflow bottleneck.

In terms of the outflow rate  $\gamma$ , the steady-state condition can be written as

$$\gamma \sim \frac{V_A}{\lambda_{\parallel}}, \quad V_{\text{rec}} \sim \gamma a \sim V_A \frac{a}{\lambda_{\parallel}}. \quad (7)$$

While the maximum linear tearing mode has a characteristic wavelength  $\sim k_{\text{max}}^{-1}$  that governs the *spacing of plasmoids*, the global reconnection rate is set by the

overall exhaust, for which the appropriate parallel scale is the system size,  $\lambda_{\parallel} \sim L$ . Substituting  $\gamma_{\max}$  (Eq. 4) with this identification yields

$$\frac{V_A}{\lambda_{\parallel}} \sim \frac{V_A}{a} S_a^{-1/2} = \frac{V_A}{a} \left( \frac{\eta}{V_A a} \right)^{1/2}, \quad (8)$$

which provides  $a$ :

$$a \sim \left( \frac{\eta \lambda_{\parallel}^2}{V_A} \right)^{1/3}. \quad (9)$$

Hence, the global *steady-state* reconnection rate becomes

$$V_{\text{rec}} \sim V_A \left( \frac{\eta}{V_A L} \right)^{1/3} \sim V_A S^{-1/3}. \quad (10)$$

Thus, evaluating the reconnection rate at the maximum tearing growth mode, but using the global parallel scale for the outflow constraint, produces the tearing-limited scaling  $V_{\text{rec}} \propto V_A S^{-1/3}$ . The internal wavenumber  $k_{\max}$  sets the number and distribution of plasmoids, whereas the global throughput remains limited by the system-length exhaust.

The derivation presented here and in Lazarian & Vishniac (1999) differs from other analyses of the tearing reconnection rate (see e.g. Loureiro et al. 2009), as it incorporates a self-consistent treatment of both the parallel and perpendicular scales of tearing—an essential requirement for achieving steady-state reconnection. In particular, Lazarian & Vishniac (1999) and the derivation above require that the perpendicular scale of tearing correspond to the parallel extent of the current sheet.

Eq. (10) resembles the Sweet–Parker prediction, as it retains an explicit dependence on the Lundquist number  $S$ , though with a slightly modified exponent. As a result, tearing-limited reconnection proceeds somewhat faster than Sweet–Parker, but still remains slow for astrophysically relevant  $S$ . Using only the FKR63 branch within the same shear-decorrelation framework gives  $V_{\text{rec}} \propto V_A S^{-3/10}$  (Lazarian & Vishniac 1999), whereas allowing the spectrum to reach the FKR–Coppi crossover (maximum growth) yields the slightly steeper  $V_{\text{rec}} \propto V_A S^{-1/3}$ . The differences between these two scalings are of secondary practical importance. In both cases the physical interpretation is the same—reconnection is limited by shear stabilization and constrained by mass conservation, with  $V_{\text{rec}} \sim V_A a / \lambda_k$ ; the only distinction is whether the growth rate is evaluated on the FKR branch or at the FKR–Coppi crossover. The transition from the Sweet–Parker scaling to the faster tearing-limited scaling of Eq. (10) is expected as soon as the current sheet becomes unstable to tearing.

### 2.3. Critical Lundquist Number for the Transition to Plasmoid-Mediated Reconnection

A Sweet–Parker (SP)current sheet of length  $L$  has half-thickness  $a_{\text{SP}} \sim LS^{-1/2}$ , corresponding to  $S_a \sim S^{1/2}$ . In such a sheet, the fastest tearing mode grows at

$$k_{\max} L \approx C_k S^{3/8}, \quad \gamma_{\max} \tau_A \approx C_{\gamma} S^{1/4}, \quad \tau_A = L/V_A. \quad (11)$$

The plasmoid instability requires that unstable modes both fit within the sheet and grow sufficiently before being advected out. The first condition,  $k_{\max} L \gtrsim 1$ , is already met at very low  $S$  and is therefore not a limiting constraint. The second condition,  $\gamma_{\max} \tau_A \gtrsim N$ , expresses that the perturbation amplitude must grow by  $N$  e-foldings<sup>2</sup> during one Alfvén crossing time. Writing the perturbation as  $A(t) = A_0 e^{\gamma t}$ , a single e-fold corresponds to amplification by a factor of  $e$ , while  $N = 5$  corresponds to a factor of  $\sim 150$ , and  $N = 10$  to  $\sim 2.2 \times 10^4$ . In practice, several e-folds are required for perturbations to rise above background noise and drive nonlinear disruption. This condition leads to the threshold

$$S_c \approx \left( \frac{N}{C_{\gamma}} \right)^4. \quad (12)$$

For  $C_{\gamma} \approx 0.5$ , this simplifies to  $S_c \approx (2N)^4$ , so that  $N = 5\text{--}10$  yields  $S_c \sim 10^4\text{--}10^5$ .

It is also important to recall the long-wavelength ordering for tearing,  $ka < 1$ , which is a prerequisite for the applicability of the linear theory. For the fastest tearing mode in a SP current sheet we have

$$k_{\max} a = (k_{\max} L) \frac{a}{L} \approx C_k S^{3/8} S^{-1/2} = C_k S^{-1/8}. \quad (13)$$

Thus the criterion  $k_{\max} a < 1$  is automatically satisfied for  $S \gg 1$ , since  $k_{\max} a$  decreases as  $S^{-1/8}$ . The corresponding bound is

$$S \gtrsim S_{ka} \equiv C_k^8, \quad (14)$$

which with  $C_k \approx 1.05$  gives  $S_{ka} \approx 1.5$ . This value is negligible compared to the thresholds implied by the growth condition. More generally, the interval of unstable wavenumbers satisfying  $L^{-1} \lesssim k \lesssim a^{-1}$  always exist for SP current sheets with  $a < L$ . Therefore, in practice, the onset of plasmoid formation is not limited by the  $ka < 1$  ordering, but by the requirement of sufficient exponential amplification.

<sup>2</sup> The “e-folding” time is the interval over which an exponentially growing or decaying quantity changes by a factor of  $e \simeq 2.718$ . The terminology is standard in astrophysics and fluid dynamics; see, e.g., Lippis (1963) or Goldsmith (1970).

Thus, the analytic estimate indicates that plasmoid-mediated reconnection should onset at  $S_c \sim 10^4\text{--}10^5$ , corresponding to several e-folds of growth within one global Alfvén time. In the next sections we will examine how this theoretical threshold compares with our numerical simulations.

### 3. NUMERICAL METHODOLOGY

#### 3.1. The code

We use the high-order shock-capturing Godunov-type code AMUN<sup>3</sup> (Kowal et al. 2009, 2012) to solve the isothermal visco-resistive 2D MHD equations:

$$\frac{\partial \rho}{\partial t} + \nabla \cdot (\rho \mathbf{v}) = 0, \quad (15)$$

$$\frac{\partial(\rho \mathbf{v})}{\partial t} + \nabla \cdot \left[ \rho \mathbf{v} \mathbf{v} + \left( p + \frac{B^2}{8\pi} \right) \mathbf{I} - \frac{1}{4\pi} \mathbf{B} \mathbf{B} \right] = \nabla \cdot \tau + \mathbf{f}, \quad (16)$$

$$\frac{\partial \mathbf{B}}{\partial t} + \nabla \times \mathbf{E} = 0, \quad (17)$$

where  $\rho$  and  $\mathbf{v}$  are the plasma density and velocity, respectively,  $\mathbf{B}$  is the magnetic field,  $\mathbf{E} = -\mathbf{v} \times \mathbf{B} + \eta \mathbf{j}$  is the electric field,  $\mathbf{j} = \nabla \times \mathbf{B}$  is the current density,  $p = \rho c_s^2$  is the thermal pressure,  $c_s$  is the isothermal sound speed,  $\eta$  is the resistivity coefficient,  $\tau = \nu \rho [\nabla \mathbf{v} + \nabla^T \mathbf{v} - \frac{2}{3} \nabla \cdot \mathbf{v}]$  is the viscous stress tensor,  $\nu$  is the kinematic viscosity, and  $\mathbf{f}$  represents the forcing term.

To numerically solve the 2D MHD set of equations, we used the HLLD Riemann solver (Mignone 2007) with a 5<sup>th</sup>-order Monotonicity-Preserving (MP5) reconstruction method (Suresh & Huynh 1997) to reconstruct the Riemann states, and a 3<sup>rd</sup>-order 4-step Embedded Strong Stability Preserving Runge-Kutta (SSPRK) method for time advance, where the time step is controlled by both the Courant-Friedrichs-Lowy (CFL) condition and the integration error (see, e.g., Ranocha et al. 2022).

The code uses dimensionless equations in such a way that the strength of the magnetic field is expressed in terms of the Alfvén velocity, which is defined by the antiparallel component of the magnetic field (reconnecting field) and the unperturbed density  $\rho_0 = 1$ . All other velocities are expressed as units of the Alfvén speed, the length of the box in the  $x$ -direction ( $L_x$ ) defines the unit of distance, and time is measured in units of the Alfvén time, defined as  $t_A \equiv L_x/V_A$ .

#### 3.2. Numerical setup

The configuration of the magnetic field in the reconnection region is similar to the one employed by Bhattacharjee et al. (2009); Huang & Bhattacharjee (2010), where the attraction between two coalescing magnetic flux tubes is the driver of magnetic reconnection. The simulation domain is a 2D square with dimensions  $L_x = L_y = L = 1$ , and the effective resolution for the simulations varies between  $512^2$  and  $32,768^2$  grid points. The reconnecting magnetic field is along the  $x$ -direction (see Fig. 1). The boundary conditions in our models are perfectly conducting, free slipping boundaries along  $x$  and  $y$  directions.

The initial magnetic field is given by  $\mathbf{B} = \hat{z} \times \nabla \psi + B_z \hat{z}$ , where

$$\psi = \frac{1}{2\pi} \tanh\left(\frac{y}{\delta}\right) \cos(\pi x) \sin(2\pi y), \quad (18)$$

and  $B_z$  is the guide field. We adopted, for our initial configuration, a constant guide field with amplitude  $B_z = 0.5$ , while the density is nonuniform to maintain the pressure balance (see Fig. 1). The initial current sheet thickness  $\delta$  is set to be  $S^{-1/2}$ , following the Sweet-Parker scaling.

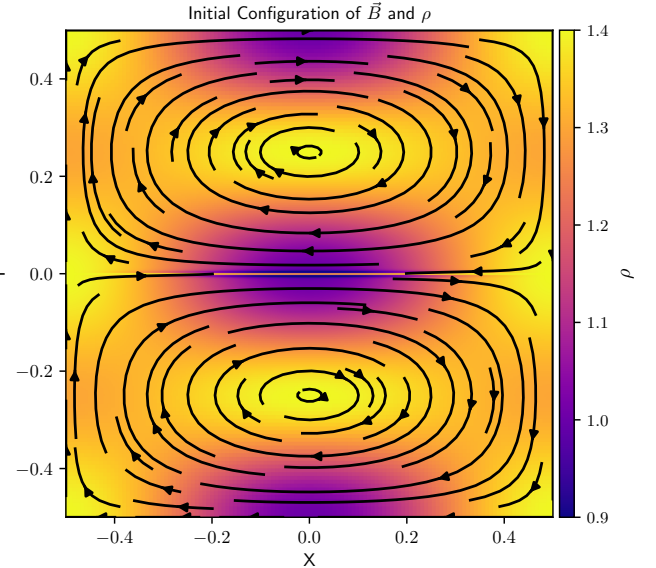


**Figure 1.** Initial configuration of magnetic field and density. Black arrows represent the in-plane component of the magnetic field, and the colormap is the density profile. The out-of-plane component of the magnetic field ( $B_z$ ) is set to be constant.

#### 3.3. Initial perturbation

We have tested two different methods to drive the initial perturbation in the system. First, we adopted an

<sup>3</sup> The code is freely available at <https://bitbucket.org/amunteam/amun-code/>.

initial Gaussian noise in the velocity field, with amplitudes of  $\delta v = \{1, 10, 100\} \times 10^{-3} V_A$ .

We also drove small-scale perturbation for a short initial period into the system. In this case, we employ a technique described by [Alvelius \(1999\)](#) (see also [Kowal et al. 2009; Kulpa-Dybel et al. 2010](#), for a detailed discussion of this method). This forcing is applied in the spectral space, concentrated around a wave vector  $k_{\text{inj}}$  that corresponds to the injection scale  $l_{\text{inj}} \sim k_{\text{inj}}^{-1}$ . Within a shell extending from  $k_{\text{inj}} - \Delta k_{\text{inj}}$  to  $k_{\text{inj}} + \Delta k_{\text{inj}}$ , we disturb  $N$  discrete Fourier components of velocity using a Gaussian profile characterized by a half-width  $k_c$  and a peak amplitude  $v_f$  at the injection scale. The amplitude of the perturbation is given by the injection power  $P_{\text{inj}}$ .

We adopted different combinations of  $k_{\text{inj}}$  and  $P_{\text{inj}}$ , but in all models tested with external forcing, the perturbation is injected into the system at the beginning of the simulation ( $t = 0$ ) up to  $t = 0.1 t_A$ . After that, the simulations evolve without external perturbation. Table 1 lists the initial conditions of the models simulated in this work.

#### 4. MEASURING THE RECONNECTION RATE

We adapt the method described by [Kowal et al. \(2009\)](#) (see also [Vicentin et al. 2025](#)) to calculate the reconnection rate from the unsigned magnetic flux. Specifically, we integrate  $|B_x|$  over  $x = 0$ , perpendicular to the current sheet. Since the signed flux through this plane is zero, dividing the unsigned integral by two gives the flux contribution from each polarity. As time evolves, the two initial flux ropes merge, and  $|B_x|$  decreases due to the reconnection process. Then, we have the reconnection rate given by the time derivative of the unsigned magnetic flux:

$$V_{\text{rec}} = -\frac{1}{2|B_{x,0}|} \frac{\partial \Phi_B}{\partial t} = -\frac{1}{2|B_{x,0}|} \frac{\partial}{\partial t} \int_{-0.5}^{0.5} |B_x| dy, \quad (19)$$

where  $|B_{x,0}|$  represents the initial amplitude of the non-reconnecting field, that in this configuration is given by  $|B_{x,0}| = \max(|B_x|_{x=0}) \sim 1$ , and  $\Phi_B$  is the unsigned magnetic flux integrated across the center of the box ( $x = 0$ ).

By adopting this method, we avoid problems caused by the accumulation of magnetic flux along the  $x$ -boundaries, since we are integrating the flux across the center of the box at  $x = 0$ .

#### 5. RESULTS

We discuss in this Section the results of 2D MHD simulations of current sheets for different values of

$S(\times 10^3)$	$h^{-1}$	Perturb.	$\delta v$	$k$
1	512	RN	$10^{-2}$	-
2	512	RN	$10^{-2}$	-
5	512	RN	$10^{-2}$	-
5	1024	RN	$10^{-2}$	-
10	512	RN	$10^{-2}$	-
10	1024	RN	$10^{-2}$	-
10	2048	RN	$10^{-2}$	-
50	512	RN	$10^{-2}$	-
50	1024	RN	$10^{-2}$	-
50	2048	RN	$10^{-2}$	-
50	4096	RN	$10^{-3}$	-
50	4096	RN	$10^{-2}$	-
50	4096	RN	$10^{-1}$	-
50	8192	RN	$10^{-2}$	-
50	8192	MM	-	60
50	8192	MM	-	128
50	8192	MM	-	256
50	8192	MM	-	1024
100	8192	RN	$10^{-2}$	-
100	16384	RN	$10^{-2}$	-
100	16384	MM	-	80
200	32768	RN	$10^{-2}$	-

**Table 1.** List of initial parameters of the simulated models. In this table,  $S = LV_A/\eta$  is the Lundquist number,  $h^{-1}$  is the inverse of the grid size,  $\delta v$  is the amplitude of the random noise (RN) perturbation, and  $k$  is the wavenumber of the multi-mode (MM) perturbation. All models have magnetic Prandtl number  $\text{Pr}_m \equiv \nu/\mu = 1$ , and the initial thickness  $\delta = S^{-1/2}$ .

Lundquist number, numerical grid resolution, and the two drivers of the initial perturbation. We also show a new method to compute the numerical error from the simulations using the components of the magnetic energy density equation.

##### 5.1. Models with initial random noise

In the absence of external forcing or instabilities, the reconnection rate measured within the current sheet should follow the Sweet-Parker dependence on the Lundquist number,  $V_{\text{rec}} \sim S^{-1/2}$ , at least until a critical Lundquist number  $S_c$  where the plasmoid instability can occur, making the reconnection rate reach a constant value, as verified, e.g., in the MHD simulations of [Bhattacharjee et al. \(2009\); Huang & Bhattacharjee \(2010\); Loureiro et al. \(2012\)](#). As stressed earlier, in these works, the authors found  $S_c \sim 10^4$ , and a “universal” rate of  $V_{\text{rec}}/V_A \sim S_c^{-1/2} \sim 0.01$ .

In the present work, for each Lundquist number tested in our simulations, we analyzed the convergence of mag-

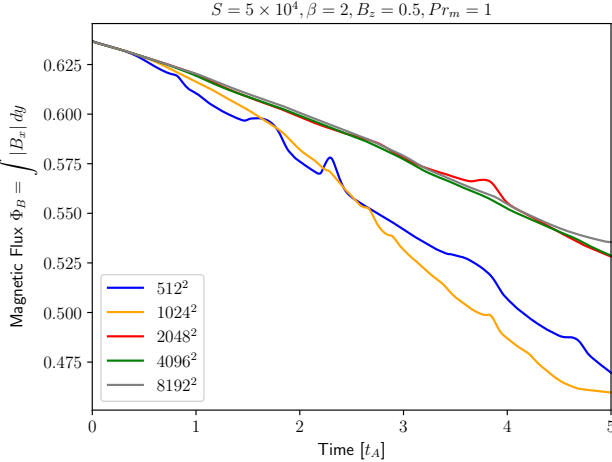


**Figure 2.** Time evolution of the magnetic flux  $\Phi_B$  for 2D MHD simulations with initial random noise perturbation,  $S = 5 \times 10^4$ ,  $\delta v = 10^{-2} V_A$  and different resolutions.

magnetic flux over time for different grid resolutions. In Fig. 2 we show the time evolution of the magnetic flux for the simulations with  $S = 5 \times 10^4$  and  $512^2 - 8192^2$  grid cells.

From Fig. 2, we observe that convergence is achieved at a resolution  $2048^2$ . In this case, the tearing-mode instability still develops, and the bump seen at time  $t \lesssim 4.0 t_A$  is attributed to the passage of a plasmoid through the center of the box ( $x = 0$ ). For higher resolutions, of  $4096^2$  and  $8192^2$ , although plasmoids still form, they are rapidly advected out of the domain (see Fig. 3 for the resolution  $h^{-1} = 8192$  and therefore do not affect the magnetic flux or the corresponding reconnection rate.

We note that, for the simulations shown in Fig. 2, the Lundquist number is  $S = 5 \times 10^4$ , which yields a current layer thickness of  $\delta \sim S^{-1/2} \approx 4.47 \times 10^{-3}$ . Using a grid resolution of  $h^{-1} = 2048$  to marginally resolve the reconnection region, we obtain a ratio of  $\delta/h \approx 9.15$ . Therefore, the convergence criterion proposed by Morillo & Alexakis (2025), which requires  $\delta/h \geq 10$ , appears to be a reasonable guideline for assessing numerical resolution for all tests with resolution 2048 or larger. However, plasmoid formation is still observed even in these cases where  $\delta/h > 10$ , in contrast to their findings.

For example, Figure 3 shows 2D colormaps of the current density magnitude ( $|\mathbf{J}| = |\nabla \times \mathbf{B}|$ ) at different snapshots of the simulation with  $S = 5 \times 10^4$  and  $h^{-1} = 8192$ . In this converged regime, plasmoids are generated but are rapidly advected out of the 2D domain without merging or evolving into “monster” plasmoids. Even when the simulation is extended to much longer timescales, the absence of growing plasmoids remains,

as demonstrated in Figure 12 in the Appendix B for a run lasting up to  $10 t_A$  with  $S = 10^5$ .

It is also worth noting that in some of our simulations we observed the propagation of waves from the domain boundaries toward the center, a consequence of the imposed closed boundary conditions (see, for example, the snapshot at  $t = 3.5 t_A$  in Fig. 3). These waves can influence the system by introducing additional perturbations, which in turn may contribute to plasmoid formation.

Figure 4 shows the time evolution of the magnetic flux for simulations with  $S = 5 \times 10^4$ , resolution  $h^{-1} = 4096$ , and different amplitudes of the initial random velocity perturbation,  $\delta v = \{10^{-3}, 10^{-2}, 10^{-1}\} V_A$ . The initial reconnection rate is  $V_{\text{rec}}/V_A = 0.008$  in all cases. The differences arise from the amplitude of the perturbation: for  $\delta v/V_A = 10^{-1}$  (red curve), the first plasmoids appear at  $t \sim 0.6 t_A$ , after which the reconnection rate increases to 0.012. For  $\delta v/V_A = 10^{-2}$  (orange), this transition occurs at  $t \sim 1.0 t_A$ , and for  $\delta v/V_A = 10^{-3}$  (blue) it is delayed until  $t \sim 2.6 t_A$ . Unless otherwise specified, we adopt  $\delta v = 10^{-2} V_A$  as the standard amplitude of the initial random perturbation.

By plotting the time evolution of the magnetic flux for the simulations with different Lundquist numbers where convergence is achieved (i.e.,  $\delta/h > 10$ ), we obtain Fig. 5. It should be noted that, for  $S = 2 \times 10^5$  (black curve), the resolution of  $h^{-1} = 32768$  only marginally resolves the current sheet. In this case, plasmoid passages interfere with the computed magnetic flux—evidenced by the small bumps in the black curve—and consequently affect the inferred reconnection rate.

Subsequently, by taking the time derivative of the curves in Fig. 5 and normalizing according to Eq. (19), we obtain the average reconnection rates as a function of the Lundquist number, shown in 6.

In Fig. 6, the simulations with  $S = 10^3$  and  $S = 2 \times 10^3$  were evolved only up to  $t_{\text{max}} = 3.0 t_A$ , as the magnetic flux decays rapidly and the two flux tubes quickly coalesce into a single structure. This coalescence reduces the reconnection rate at later times. For these cases, we averaged the reconnection rate over the interval  $0 \leq t \leq 2.0 t_A$ . For  $S = 5 \times 10^3$ , the averaging was performed over  $1.0 t_A \leq t \leq 3.0 t_A$ , while for all higher- $S$  simulations the interval was  $3.0 t_A \leq t \leq 5.0 t_A$ .

From Fig. 6, we observe a good agreement between the measured reconnection rates and the Sweet–Parker scaling,  $V_{\text{rec}}/V_A \sim S^{-1/2}$  (black dashed line) for the Lundquist numbers up to  $S \sim 2 \times 10^4$ . For higher values,  $S \geq 5 \times 10^4$ , the reconnection rates deviate from the slow Sweet–Parker regime due to the development of plasmoids. In this regime, the rates are slightly en-

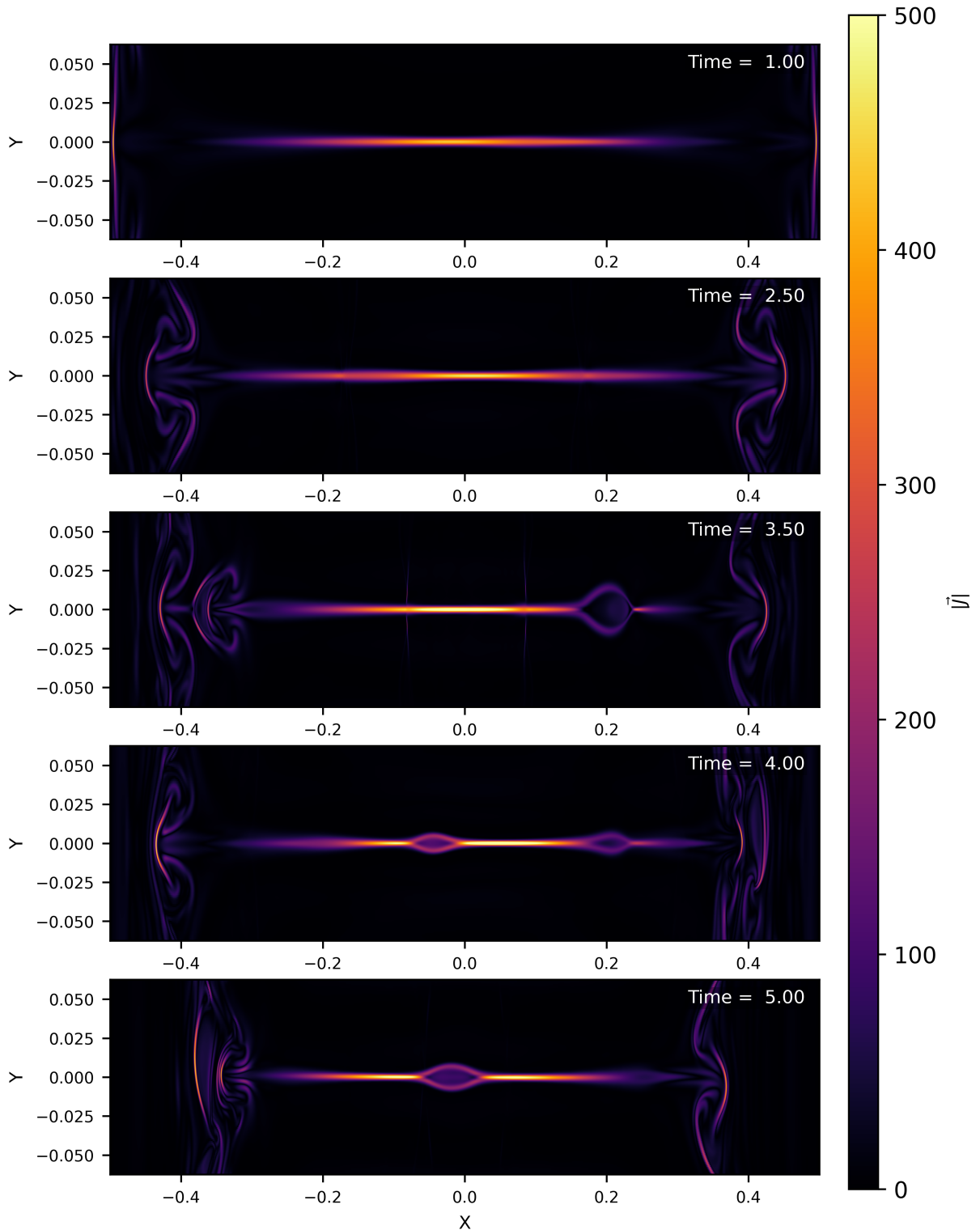


**Figure 3.** Colormaps of the current density magnitude ( $|\mathbf{J}| = |\nabla \times \mathbf{B}|$ ) at different time-steps for the simulation with  $S = 5 \times 10^4$  and  $h^{-1} = 8192$ .

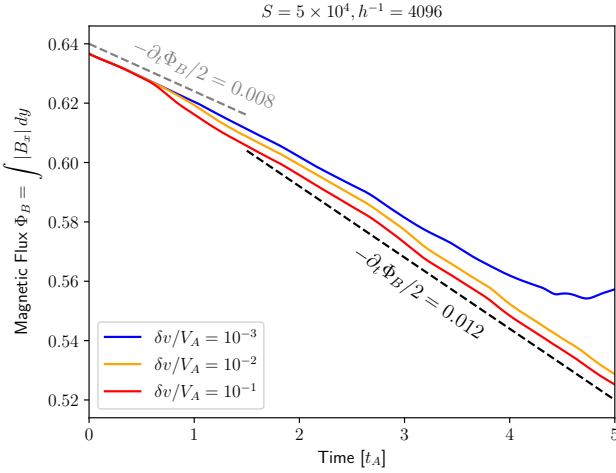


**Figure 4.** Time evolution of the magnetic flux  $\Phi_B$  for simulations with initial random noise perturbation,  $S = 5 \times 10^4$ ,  $h^{-1} = 4096$ , and different amplitudes of initial random noise  $\delta v$ .

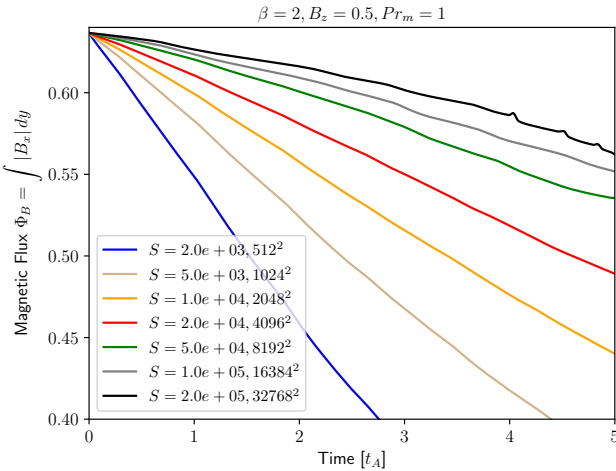


**Figure 5.** Time evolution of the magnetic flux  $\Phi_B$  for simulations with initial random noise perturbation and different Lundquist numbers at their respective best resolutions.

hanced but still depend on the Ohmic resistivity and Lundquist number, following  $V_{\text{rec}}/V_A \sim S^{-1/3}$  (orange dashed line), and thus remain slow. Remarkably, this  $S^{-1/3}$  scaling is the same as the one obtained in Section 2 (eq. 10) from linear theory of reconnection driven by tearing mode.<sup>4</sup>

### 5.2. Models with multi-mode small-scale initial perturbation

As pointed out earlier, we adopted two different methods to drive the initial perturbation into the 2D domain. In this section, we discuss the results of the simulations with multi-mode, small-scale ( $k \gg 1$ ) initial perturbation (see, e.g., Alvelius 1999; Kowal et al. 2009; Kuppa-Dybel et al. 2010).

In Fig. 7, we present the time evolution of the magnetic flux for the simulations with  $S = 5 \times 10^4$  and  $h^{-1} = 8192$ . Except for the blue curve, which corresponds to a model initialized with random noise (as in Fig. 5), all other simulations in Fig. 7 were perturbed using small-scale, multi-mode fluctuations peaked around a wavenumber  $k$  and injected over a short interval (from  $t = 0$  up to  $0.1 t_A$ ). We find that perturbations at scales of  $\ell \sim k^{-1}$  are close to the resistive scale of the simulation, making them effective at triggering small-scale instabilities such as the tearing mode. The modes satisfy  $|\mathbf{k}| = k$ , but with the constraint  $k_x < (2\pi\delta)^{-1}$ , where  $\delta$  is the initial current sheet thickness.

Despite small variations in the curves, primarily caused by the passage of plasmoids through the center of the domain, all runs are consistent with a nearly constant reconnection rate of  $V_{\text{rec}}/V_A \sim 0.012$ , comparable to the value obtained for the model initialized with random noise (blue curve, see also Figure 6). This result is also in agreement with the scaling  $V_{\text{rec}} \propto S^{-1/3}$  predicted for tearing mode-driven reconnection.

In Fig. 8, we present the same analysis for simulations with  $S = 10^5$  and two initial perturbations: random noise with  $\delta v = 10^{-2} V_A$  (blue), and a multi-mode perturbation with  $k = 80$  (orange). In both cases the system reaches the same average reconnection rate  $\langle V_{\text{rec}} \rangle = 0.009 V_A$  which is also consistent with the tearing-mode-driven reconnection scale  $V_{\text{rec}} \propto S^{-1/3}$ .

### 5.3. Error estimation

Although significant efforts have explored magnetic reconnection in the high-Lundquist-number regime, systematic convergence studies and quantitative evaluations of numerical error remain scarce. If the increase of the Lundquist number  $S$  is achieved by decreasing the resistivity  $\eta$ , the current sheet becomes extremely thin, with its initial laminar thickness scaling as  $\delta \sim \eta^{1/2} \sim S^{-1/2}$ , under the Sweet-Parker model, thereby requiring very high spatial resolution for accurate representation. Without rigorous error quantification, it is challenging to determine whether reported results reflect genuine physical behavior or are affected by artifacts introduced by insufficient numerical resolution. In this section we present a method to estimate the errors of our analysis.

<sup>4</sup> We also note that the difference between the  $S^{-1/3}$  scaling and the one obtained in Lazarian & Vishniac 1999,  $S^{-3/10}$  (see eq. 6), is insignificant and well within the numerical errors.

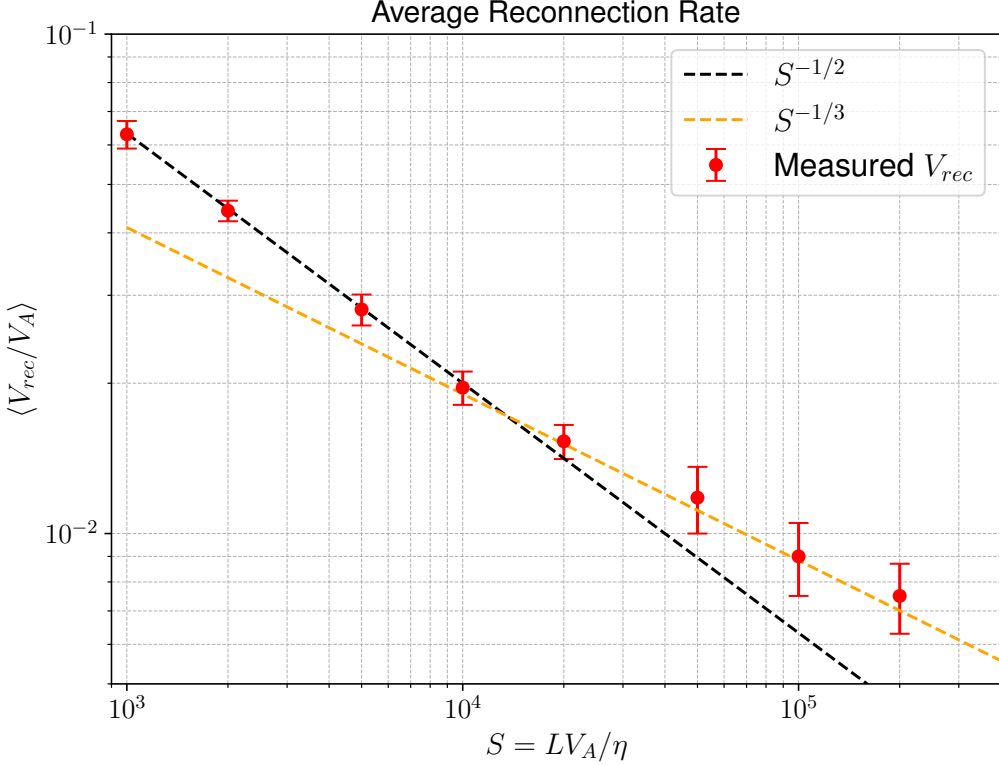


**Figure 6.** Dependence of the average reconnection rate  $V_{rec}$  on the Lundquist Number  $S$  for models with initial random noise perturbation. The dashed black line represents the Sweet-Parker scaling of  $V_{rec} \propto S^{-1/2}$ , and the orange dashed line represents the scaling for the linear tearing mode-mediated reconnection  $V_{rec} \propto S^{-1/3}$  – as in Eq. (10).

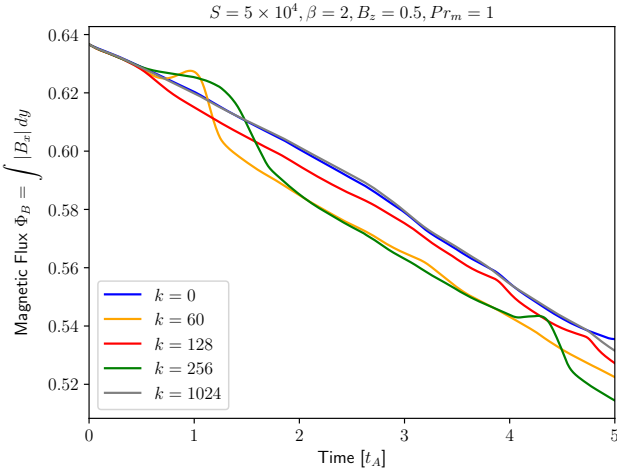


**Figure 7.** Magnetic flux evolution for the simulations with initial small-scale perturbation,  $S = 5 \times 10^4$  and resolution  $h = 1/8192$ . The colors represent different wavenumbers of the initial perturbation, injected from  $t = 0$  up to  $0.1 t_A$ . The only exception is the blue curve, which was obtained using initial random noise as in Figures 2 to 6, and is shown here for comparison.

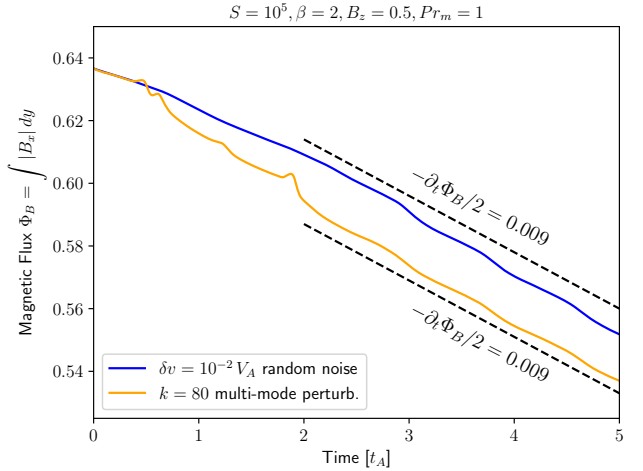


**Figure 8.** Magnetic flux evolution for the simulations with initial random noise ( $\delta v = 10^{-2} V_A$ , blue) and small-scale ( $k = 80$ , orange) perturbation,  $S = 1 \times 10^5$  and resolution  $h = 1/16384$ . The dashed black line corresponds to  $V_{rec} = 0.009 V_A$ , the average reconnection rate measured in  $2.0 \leq t \leq 5.0 t_A$ .

In resistive MHD, the time evolution of the magnetic energy density  $E_B$  is governed by the volumetric integral equation:

$$\begin{aligned} \frac{dE_B}{dt} = & - \iiint_V (\vec{v} \times \vec{B}) \cdot \vec{J} dV - \iiint_V \eta |\vec{J}|^2 dV \\ & + \iint_{\partial V} [\vec{E} \times \vec{B}] \cdot \hat{n} dS, \end{aligned} \quad (20)$$

where  $E_B \equiv \iiint_V \frac{1}{2} |\vec{B}|^2 dV$  is the magnetic energy integrated across the entire simulated box, and the Poynting flux  $\iint_{\partial V} [\vec{E} \times \vec{B}] \cdot \hat{n} dS$  vanishes due to the boundary conditions imposed. Therefore, we can estimate the numerical error from the components of the Eq. (20), by assuming

$$\epsilon = \left| \frac{dE_B}{dt} + \iiint_V (\vec{v} \times \vec{B}) \cdot \vec{J} dV + \iiint_V \eta |\vec{J}|^2 dV \right|. \quad (21)$$

In Fig. 9 (left) we show the time evolution of all components of Eq. (21) along with the estimated numerical error,  $\epsilon$  (black solid line), for the simulation with  $S = 5 \times 10^4$  and  $h^{-1} = 512$ . For this low resolution case, the numerical error is significant and sometimes even exceeds the amplitude of the heating term ( $\eta \mathbf{J}^2$ , purple line). This indicates that, at this resolution, the simulation is not well resolved, which is consistent with the convergence analysis presented in Fig. 2.

Repeating the same analysis for the higher resolution  $h^{-1} = 8192$ , we obtain Fig. 9 (right). In this case, the numerical error  $\epsilon$  is significantly reduced and remains smaller than each individual component of the magnetic terms (in magnitude), demonstrating that the simulation is well resolved at this resolution.

In Fig. 10, we present the numerical error estimate computed from Eq. (21) for simulations with  $S = 5 \times 10^4$  and different resolutions, ranging from  $h^{-1} = 512$  to 8192. We find that convergence is achieved for the highest resolutions,  $h^{-1} = 4096$  and 8192, where the condition  $\delta/h > 18$  is satisfied, which is even more stringent than the threshold reported by Morillo & Alexakis (2025).

For Figures 4 — 8, we not only considered simulations satisfying the Morillo & Alexakis (2025) criterion of  $\delta/h > 10$ , but also analyzed the convergence of the magnetic flux and the numerical error estimated from Eq. (21). In these figures, the average reconnection rates were obtained from simulations where the numerical error  $\epsilon$  converged and was smaller than the magnitudes of each magnetic term in Eq. (21).

## 6. DISCUSSION

### 6.1. Previous Studies of Tearing-Driven Reconnection

Numerical investigations of magnetic reconnection mediated by the tearing mode have, for decades, been

primarily limited to two-dimensional simulations (see, e.g., Matthaeus & Lamkin 1985; Biskamp 1986; Uzdensky & Kulsrud 2000; Samtaney et al. 2009; Daughton et al. 2009; Loureiro et al. 2009; Bhattacharjee et al. 2009; Huang & Bhattacharjee 2010; Loureiro et al. 2012; Comisso et al. 2015, and references therein). These studies generally indicated that once the Lundquist number exceeds a critical value of  $S_c \sim 10^4$ , plasmoids emerge, interact, and grow, altering the topology of the current sheet and stabilizing the reconnection rate at a so-called “universal” value,  $V_{\text{rec}}/V_A \approx S_c^{-1/2} \approx 0.01$ .

More recent work, however, has challenged this picture. Morillo & Alexakis (2025), using high-resolution Orszag–Tang vortex simulations, reported no plasmoids up to  $S = 5 \times 10^5$ . They argued that when the criterion  $\delta/h > 10$  is satisfied—where  $\delta$  is the sheet thickness and  $h$  the grid cell size—plasmoid formation is suppressed, and the reconnection rate continues to follow the Sweet–Parker scaling, remaining resistivity dependent and therefore slow. On the other hand, the tearing instability is a genuine physical process and should not depend on numerical resolution alone. Indeed, Huang et al. (2017) demonstrated that in highly controlled setups with extremely low noise amplitudes ( $\epsilon = 10^{-30}$ ), the critical Lundquist number can increase to  $S_c \sim 10^6$ . This suggests that the absence of plasmoids in Morillo & Alexakis (2025) is more likely a consequence of the extremely quiet numerical environment rather than a genuine suppression of tearing.

These contrasting results highlight the need for simulations that combine high resolution with a controlled level of perturbations and include systematic convergence analyses, which earlier works generally lacked.

### 6.2. New Insights into Tearing-Driven Reconnection

In this work, we performed simulations of high-Lundquist-number current sheets, in which the tearing mode instability can develop. In such regimes, the sheet thickness decreases as  $\delta \sim \eta^{1/2}$  with resistivity, requiring increasingly fine resolution as  $\eta$  decreases.<sup>5</sup>

To quantify numerical accuracy, we developed a new convergence method based on the full evolution equations of magnetic flux and magnetic energy. By estimating all contributing terms and comparing their sum with the corresponding time derivatives, we directly evaluated the numerical error. This analysis established that the resolution threshold  $\delta/h > 10$  is indeed required

<sup>5</sup> This setup is relevant to numerical simulations but not directly to astrophysical plasmas, where  $\eta$  is fixed by plasma parameters and  $S$  grows instead with the macroscopic length scale  $L$  (see Sec. 6.4).

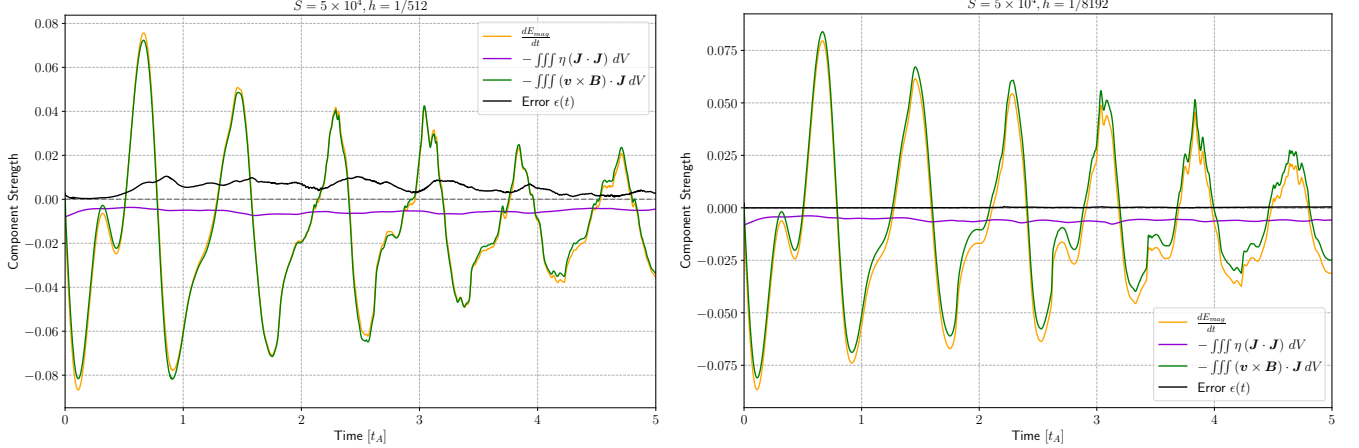


**Figure 9.** Components of the Eq. (20) and numerical error estimation (black solid line) from Eq. (21) for the simulation with initial random noise,  $S = 5 \times 10^4$  and  $h = 1/512$  (left) and  $h = 1/8192$  (right).

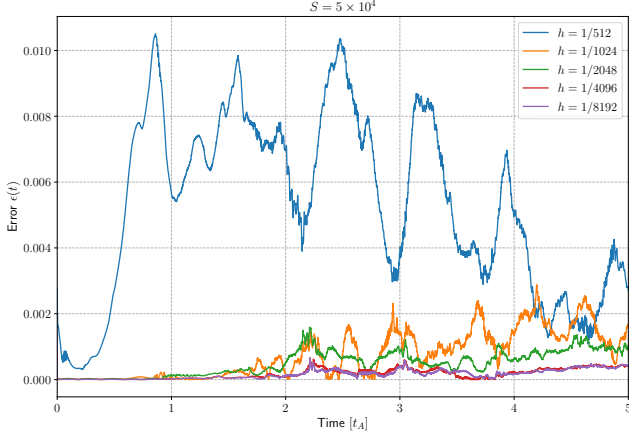


**Figure 10.** Numerical error estimate calculated from Eq. (21) for simulations with initial random noise,  $S = 5 \times 10^4$  and different resolutions.

to resolve the current sheet thickness, consistent with the criterion of Morillo & Alexakis (2025), but here confirmed through explicit energy-balance tests. Importantly, we introduced random noise into our simulations, thereby ensuring that insufficient perturbations do not artificially suppress tearing. As a result, we clearly observe the onset of tearing instability in well-resolved runs.

Our simulations reveal that plasmoid formation sets in only for  $S \gtrsim 5 \times 10^4$ . Beyond this threshold, the reconnection rate is enhanced relative to the Sweet–Parker prediction,  $V_{\text{rec}} \sim S^{-1/2}$ , but does not saturate to a constant. Instead, it remains Lundquist dependent, following a slower scaling  $V_{\text{rec}} \sim S^{-1/3}$ , as predicted by linear tearing theory (Eq. 10) and consistent with analytical expectations (e.g., Lazarian & Vishniac 1999).

Thus, even in the plasmoid-unstable regime, our very high-resolution simulations show reconnection rates be-

low the often-cited  $0.01V_A$  for  $S > 5 \times 10^4$  (Fig. 6). This result cautions against interpreting a measured rate of  $0.01V_A$  as evidence of convergence, as has sometimes been assumed in the literature. Smaller, Lundquist-dependent rates can persist even at high resolution, indicating that two-dimensional tearing-driven reconnection does not yield a truly universal fast rate.

### 6.3. Limitations of the Present Study

Our findings establish a new  $S^{-1/3}$  regime of two-dimensional tearing reconnection that spans a broad range of Lundquist numbers. Nevertheless, they do not rule out the existence of other regimes at even higher  $S$ . What our results do show is that earlier claims of a universal threshold at  $S \approx 10^4$  were not numerically robust, since they were based on insufficiently resolved current sheets.

Furthermore, our study is limited to resistive MHD in two dimensions. Additional plasma processes—such as anomalous resistivity, pressure anisotropy or kinetic effects—may alter the onset and growth of tearing, either suppressing or enhancing reconnection rates (e.g., Otto 1991; Birk & Otto 1991; Büchner 2006; Huang et al. 2013; Chiou & Hau 2002, 2003; Ferreira-Santos et al. 2025; Shay et al. 1999; Yamada et al. 2010; Shi et al. 2020; Mirnov et al. 2004; Hosseinpour et al. 2009; Meshcheriakov et al. 2012). Whether such microphysical effects persist at macroscopic scales remains uncertain. More importantly, reconnection in astrophysical environments is inherently three-dimensional: flux ropes can interact, merge, and drive turbulence, leading to reconnection dynamics that cannot be captured in 2D.

Finally, our convergence analysis and numerical error estimation method are themselves restricted in scope. By construction, the method evaluates errors through the resistive MHD magnetic flux and magnetic energy

evolution equations. While this provides a rigorous test in 2D and 3D non-ideal single-fluid MHD, its direct applicability to multi-fluid or kinetic simulations is limited, as additional terms and energy channels come into play. Extending such error estimation techniques to more complex plasma descriptions remains an important task for future work.

#### 6.4. Applicability to Astrophysical Reconnection

The direct applicability of our results to astrophysical environments is limited, since magnetic reconnection in two and three dimensions differs fundamentally. In particular, we will show below that the expected Reynolds numbers of the reconnection outflow are so high that the onset of a turbulent regime is inevitable.

In numerical simulations, the Lundquist number  $S$  is increased by decreasing the resistivity  $\eta$ , while in astrophysical plasmas  $\eta$  remains essentially constant and  $S$  grows with the macroscopic system size  $L$ . This distinction has important consequences. Mass conservation requires

$$\delta \approx L \frac{V_{\text{rec}}}{V_A}, \quad (22)$$

so that the thickness of the outflow depends directly on the reconnection regime. Substituting reconnection scalings, we obtain

$$V_{\text{rec,SP}} \sim V_A S^{-1/2}, \quad \delta_{\text{SP}} \sim L S^{-1/2}, \quad (23)$$

$$V_{\text{rec,TM}} \sim 0.01 V_A \left( \frac{S}{10^4} \right)^{-1/3}, \quad \delta_{\text{TM}} \sim L S^{-1/3}, \quad (24)$$

corresponding, respectively, to the Sweet–Parker regime (SP) and the tearing-mediated (TM) regime the existence of which we confirmed numerically.

We have found that the regime described by Eq. (24), which starts for  $S \simeq 10^4$ , remains valid up to the maximum Lundquist number tested in this study ( $S = 2 \times 10^5$ ). However, we cannot exclude the possibility that at higher  $S$ , two-dimensional plasmoids could trigger the merging cascade reported in previous simulations, where the reconnection layer was insufficiently resolved, ultimately leading to  $S$ -independent reconnection. Assuming, hypothetically, that the regime of resistivity-independent tearing reconnection can be observed in future simulations with well-resolved reconnection layer at Lundquist numbers  $S_{\text{fast}} > 2 \times 10^5$ , one can write the corresponding hypothetical 2D  $S$ -independent tearing reconnection regime speed and thickness as

$$V_{\text{rec,fast}} \lesssim 0.01 V_A, \quad \delta_{\text{fast}} \sim L, \quad (25)$$

The relations above can be expressed in a unified way as

$$\delta \sim L S^{-\alpha}, \quad V_{\text{rec}} \sim V_A S^{-\alpha}, \quad (26)$$

with  $\alpha = 1/2$  for Sweet–Parker,  $\alpha = 1/3$  for tearing, and  $\alpha = 0$  for an  $S$ -independent regime.

From this scaling, the outflow Reynolds number (at the scale of the current sheet thickness  $\delta$ ) is

$$Re = \frac{V_A \delta}{\nu} \approx \frac{V_{\text{rec}}}{V_A} Pr_m^{-1} S, \quad (27)$$

where  $Pr_m = \nu/\eta$  is the magnetic Prandtl number. For Sweet–Parker reconnection,

$$Re_{\text{SP}} \sim Pr_m^{-1} S^{1/2}, \quad S < 10^4, \quad (28)$$

for the tearing-mediated regime,

$$Re_{\text{TM}} \sim Pr_m^{-1} S^{2/3}, \quad S \geq 10^4, \quad (29)$$

and for the hypothetical fast regime,

$$Re_{\text{fast}} \sim 0.01 Pr_m^{-1} \left( \frac{S_{\text{fast}}}{2 \times 10^5} \right) S, \quad S > S_{\text{fast}}. \quad (30)$$

Thus, for astrophysical plasmas where  $S$  can reach  $10^{10}$ – $10^{20}$ , one inevitably finds  $Re \gg 1$ , ensuring strongly turbulent outflows<sup>6</sup>. This agrees with arguments by Lazarian et al. (2020) that reconnection in realistic astrophysical conditions cannot remain laminar (see more details in Lazarian et al. 2025).

The presence of turbulence fundamentally changes reconnection. In 3D, turbulence alone—even without tearing—drives reconnection at a rate independent of resistivity (Lazarian & Vishniac 1999; Kowal et al. 2009; Huang & Bhattacharjee 2016; Beresnyak 2016; Kowal et al. 2017; Beg et al. 2022; Vicentin et al. 2025). Such turbulent reconnection relies on field-line wandering induced by Alfvénic modes, which are absent in 2D MHD. Therefore, 2D studies of turbulent effects are not adequate, and any resistivity-independent regime discovered in 2D would not directly apply to astrophysical settings.

Consequently, while our 2D simulations shed new light on tearing-driven reconnection and demonstrate a revised scaling regime, their direct astrophysical applicability is limited. At the large Lundquist numbers relevant to astrophysics, reconnection outflows are inevitably turbulent, and only fully three-dimensional studies can capture the interplay between tearing and turbulence that determines the true reconnection rate.

<sup>6</sup> The magnetic Prandtl number  $Pr_m$  depends on the medium’s magnetization. Since viscosity in the reconnection outflow is limited by the Bohm diffusion bound,  $\nu < r_L v_{th}$  (with  $r_L$  the ion Larmor radius and  $v_{th}$  the ion thermal speed), typical magnetized astrophysical plasmas have  $Pr_m < 1$ .

## 7. CONCLUSIONS

Despite the large body of previous work devoted to 2D magnetic reconnection in the high-Lundquist-number regime, there has been a notable lack of systematic convergence studies and quantitative estimations of numerical errors. When the Lundquist number  $S$  is increased by reducing the resistivity  $\eta$ , since  $S \sim \eta^{-1}$ , the current sheet becomes extremely thin, with its initial laminar thickness scaling according to the Sweet–Parker model as  $\delta \sim \eta^{1/2}$ . This demands extremely high numerical resolution for the current sheet to be accurately resolved. Without careful error estimation and convergence analysis, it is unclear to what extent previously reported reconnection results reflect physical reality or numerical artifacts.

In this work, we carried out very high-resolution 2D MHD simulations of reconnection layers at Lundquist numbers ranging from  $10^3$  to  $2 \times 10^5$ , where tearing instabilities can arise. We also introduced a new method to estimate numerical errors directly from the magnetic energy balance equation, allowing us to distinguish between genuine physical behavior and artifacts of discretization.

Our simulations clearly confirm the theoretical prediction for the onset of plasmoid instability. For  $Pr_m = 1$ , we observe the transition from the Sweet–Parker scaling of the reconnection rate to a tearing-dominated regime at  $S_c \simeq 1.5 \times 10^4$ . This value corresponds to about 5–6 e-foldings of growth of the fastest tearing mode within one Alfvén crossing time, in excellent agreement with the analytic criterion  $S_c \approx (N/C_\gamma)^4$  derived in Sec. 2.3. The quantitative match between simulations and analysis demonstrates the robustness of the growth–before–advection condition as the controlling factor for plasmoid-mediated reconnection.

Above this threshold, the current sheet fragments into plasmoids and the reconnection rate departs from the Sweet–Parker scaling. Importantly, unlike several earlier reports of an  $S$ -independent reconnection rate in the plasmoid regime (e.g., Loureiro et al. 2007; Bhattacharjee et al. 2009; Huang & Bhattacharjee 2010), our converged simulations do *not* exhibit saturation. Instead, when secondary current sheets are properly resolved and numerical errors are rendered insignificant, the reconnection rate follows the tearing-limited prediction (Eq. 10),

$$\frac{V_{\text{rec}}}{V_A} \sim S^{-1/3}, \quad (31)$$

consistent with Lazarian & Vishniac (1999, and references therein). This indicates that, within resistive MHD at  $Pr_m = 1$ , plasmoid-mediated reconnection re-

tains a finite dependence on  $S$  and therefore remains slow.

The main results of our numerical study can be summarized as follows:

1. We demonstrate that a resolution threshold of  $\delta/h > 10$  (where  $h$  is the grid cell size) is necessary to ensure numerical convergence of the magnetic flux. This criterion, originally suggested by Morillo & Alexakis (2025), is validated and extended in our work through systematic grid refinement and a new quantitative error estimation method based on the magnetic energy density balance (Sec. 5.3). Our analysis shows that only when this convergence requirement is satisfied, the reconnection rates reflect genuine physics rather than numerical artifacts. This result emphasizes the critical importance of rigorous convergence checks in reconnection studies.
2. The reconnection rate exhibits two distinct regimes as a function of the Lundquist number. For  $S \lesssim 2 \times 10^4$ , the reconnection rate follows the classical Sweet–Parker scaling,  $V_{\text{rec}} \sim S^{-1/2}$ , consistent with long-established theoretical predictions (Sweet 1958; Parker 1957). For higher values,  $S \gtrsim 5 \times 10^4$ , the tearing instability sets in, and plasmoids are generated. In this regime, the reconnection rate departs from the Sweet–Parker law, but does not saturate to an  $S$ -independent value. Instead, it follows the tearing-limited scaling  $V_{\text{rec}} \sim S^{-1/3}$  (Eq. 10), in agreement with earlier theoretical expectations (Lazarian & Vishniac 1999). This finding directly contradicts earlier reports of a “universal” fast rate of  $0.01 V_A$  in the plasmoid-unstable regime (e.g., Bhattacharjee et al. 2009; Huang & Bhattacharjee 2010), and shows that reconnection remains resistivity-dependent and therefore slow, even when plasmoids form.
3. For  $S \gtrsim 5 \times 10^4$ , the tearing instability becomes dynamically important and plasmoids form, even when the simulations satisfy the resolution criterion  $\delta/h > 10$ . This contradicts the claim by Morillo & Alexakis (2025) that plasmoid formation is suppressed in well-resolved simulations. Our results suggest instead that the absence of plasmoids in those studies is most likely due to insufficient perturbations to trigger the instability, rather than to a fundamental suppression of tearing. This demonstrates that tearing instability is a genuine physical process that cannot be removed simply by increased numerical resolution.

4. Although plasmoids do form above the critical Lundquist number, they are rapidly advected out of the current sheet and do not undergo successive mergers into large “monster” plasmoids, as proposed in earlier works (e.g., [Uzdensky et al. 2010](#); [Loureiro et al. 2012](#)). This absence of a plasmoid coalescence cascade further distinguishes our results from earlier reports, underscoring that in 2D the reconnection layer does not develop long-lived plasmoid chains.

Our estimates further indicate that advancing 2D studies of reconnection to higher values of  $S$  would require grid resolutions on the order of  $65,000^2$  cells or higher. This highlights both the computational challenges and the importance of performing systematic convergence analyses and quantitative error assessments in future numerical investigations of tearing-mediated reconnection.

This work also carries broader implications for reconnection studies:

- Earlier reports of resistivity-independent plasmoid reconnection in 2D MHD are likely artifacts of insufficient resolution, where numerical diffusion sets the effective current sheet thickness and artificially produces saturation.
- Even if future simulations show that 2D reconnection becomes resistivity-independent for  $S > 2 \times 10^5$ , the resulting rate would remain below  $0.01 V_A$ , i.e., still slower than the often-quoted “universal” value.
- As stressed in Section 6.4, in realistic astrophysical systems, the Reynolds number of the outflow increases as  $Re \sim Pr_m^{-1} S^{1-\alpha}$  with  $\alpha \in [0, 1/2]$ . For high  $S$ , this implies  $Re \gg 1$ , ensuring that reconnection occurs in a turbulent regime. Since turbulence fundamentally alters reconnection and behaves differently in 2D and 3D (see [Lazarian & Vishniac 1999](#); [Kowal et al. 2009](#); [Lazarian et al. 2020](#)), 2D studies cannot directly clarify the properties of high- $S$  astrophysical reconnection.
- Our results strengthen the conclusion that in astrophysical settings, where turbulence is ubiquitous, fast reconnection is more likely governed by turbulence-driven mechanisms rather than purely by the plasmoid instability.

Future studies should extend the investigation of tearing-mediated reconnection into the regime of even higher Lundquist numbers, while also moving beyond

the 2D approximation to high-resolution 3D simulations. Only then will it be possible to fully address the interplay between plasmoid instability, secondary current sheet formation, and turbulence, and to establish the conditions under which reconnection becomes truly fast in astrophysical environments.

<sup>1</sup> GHV and EMdGDP acknowledge support from the  
<sup>2</sup> Brazilian Funding Agency FAPESP (grants 2013/10559-  
<sup>3</sup> 5, 2020/11891-7, 2021/02120-0, and 2023/10590-1),  
<sup>4</sup> EMdGDP also acknowledges support from CNPq  
<sup>5</sup> (grant 308643/2017-8). GK acknowledges support  
<sup>6</sup> from FAPESP (grants 2013/10559-5, 2021/02120-0,  
<sup>7</sup> 2021/06502-4, and 2022/03972-2). AL acknowledges  
<sup>8</sup> NSF grant AST 2307840. EMdGDP also acknowledges  
<sup>9</sup> partial support by grant no. NSF PHY-2309135 to the  
<sup>10</sup> Kavli Institute for Theoretical Physics (KITP) and the  
<sup>11</sup> fruitful discussions during her stay there. The simu-  
<sup>12</sup> lations presented in this work were performed using the  
<sup>13</sup> clusters of the Group of Plasmas and High-Energy As-  
<sup>14</sup> trophysics at IAG-USP (GAPAE), and of the Group  
<sup>15</sup> of Theoretical Astrophysics at EACH-USP (Hydra), ac-  
<sup>16</sup> quired with support from FAPESP (grants 2013/10559-  
<sup>17</sup> 5, 2021/02120-0, and 2013/04073-2).

## APPENDIX

## A. CONFIRMATION OF THE SCALING OF THE MAXIMUM GROWTH RATE AND WAVENUMBER

In this Appendix, we present a numerical confirmation of the scaling relations for the maximum growth rate and the corresponding wavenumber of the linear tearing instability. Starting from the incompressible visco-resistive MHD equations, the system can be linearized, yielding the coupled equations for the  $z$ -components of velocity and magnetic field perturbations (Tenerani et al. 2015):

$$\gamma (\hat{u}'' - k^2 \hat{u}) = ik \left[ B_0 (\hat{b}'' - k^2 \hat{b}) - B_0'' \hat{b} \right] + \nu (\hat{u}''' - 2k^2 \hat{u}'' + k^4 \hat{u}) \quad (\text{A1})$$

$$\gamma \hat{b} = ik B_0 \hat{u} + \eta (\hat{b}'' - k^2 \hat{b}) \quad (\text{A2})$$

where  $\gamma$  is the growth rate,  $k$  is the wavenumber,  $\hat{u}$  and  $\hat{b}$  are the velocity and magnetic field perturbations, respectively, and  $\nu$  and  $\eta$  denote viscosity and resistivity. Primes indicate derivatives with respect to  $z$  (first, second, and fourth order, respectively). The local Lundquist number is defined as  $S_a = V_A a / \eta$ , with  $\tau_a = a / V_A$  the Alfvén time.

The equilibrium is chosen to be the force-free Harris current sheet with magnetic field

$$\mathbf{B}_0 = B_0(z) \hat{\mathbf{i}} + B_g(z) \hat{\mathbf{j}}, \quad (\text{A3})$$

where  $B_0(z) = \tanh(z/a)$  and  $B_g(z) = \text{sech}(z/a)$ , such that  $|\mathbf{B}_0|^2 = 1$ . The current sheet half-thickness  $a$  is taken as the unit length, and the equilibrium velocity is zero everywhere. This choice ensures that both the reconnecting and guide field components are present, while the total magnetic field strength remains constant.

To solve the eigenvalue problem defined by Eqs. (A1)–(A2), we used the *Pseudo-Spectral Eigenvalue Calculator with an Automated Solver* (PSECAS) framework (Berlok & Pfrommer 2019). Perturbations were expanded in normal modes, reducing the problem to a set of ODEs in  $z$ , discretized with a pseudo-spectral collocation method on a non-uniform grid optimized to resolve the steep gradients near the current sheet center. The eigenvalue problem was solved iteratively, with resolution increased until convergence of growth rates was achieved. The golden section search algorithm was applied to determine the maximum growth rate, with wavenumber relative tolerance set to  $10^{-4}$  and growth rate absolute and relative tolerances set to  $10^{-8}$  and  $10^{-4}$ , respectively.

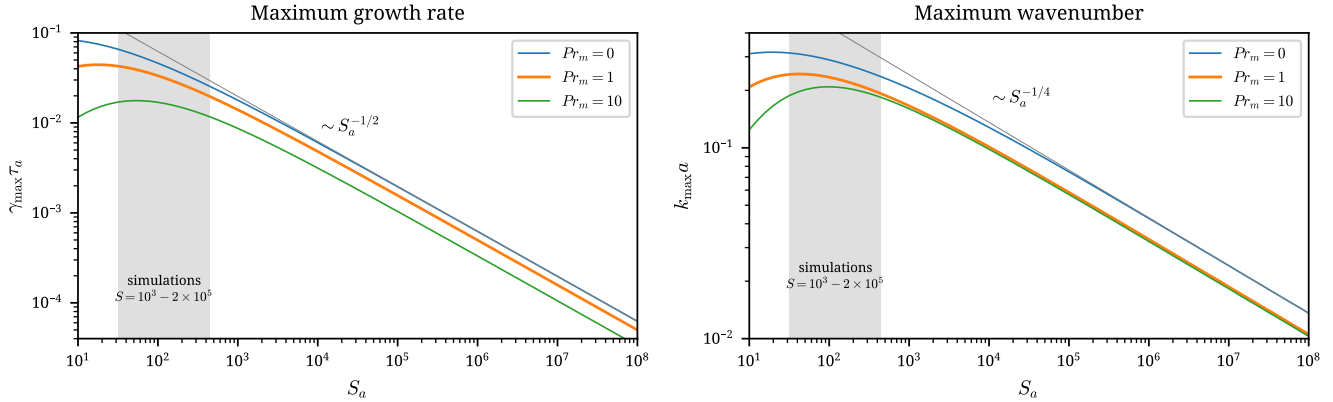


**Figure 11.** Maximum growth rate (left) and corresponding wavenumber (right) of the tearing instability as a function of Lundquist number  $S_a$  in the range  $10^1 \leq S_a \leq 10^8$ , computed with PSECAS for different Prandtl numbers. The shaded region marks the  $S_a$  ( $S_a = S^{1/2}$ ) interval covered in the simulations presented in this work. The grey line shows the analytical scalings, and fitted coefficients  $C_\gamma$  and  $C_k$  for all Prandtl numbers are reported in the text.

Figure 11 shows the maximum growth rate  $\gamma_{\max}$  (left panel) and the corresponding wavenumber (right panel) as a function of  $S_a$  for several values of the magnetic Prandtl number,  $Pr_m = \nu / \eta$ . The shaded region indicates the range of  $S_a$  values covered by our direct numerical simulations in the main part of the paper. From the fits to the high- $S_a$

results we obtained the scaling coefficients  $C_\gamma$  and  $C_k$  corresponding to the analytical predictions for  $\gamma_{\max}\tau_a \simeq C_\gamma S_a^{-1/2}$  and  $k_{\max}a \simeq C_k S_a^{-1/4}$ . The fitted coefficients are

$$\begin{aligned} Pr_m = 0 : \quad & C_\gamma = 0.623, \quad C_k = 1.360, \\ Pr_m = 1 : \quad & C_\gamma = 0.499, \quad C_k = 1.053, \\ Pr_m = 10 : \quad & C_\gamma = 0.333, \quad C_k = 1.029. \end{aligned}$$

For the case  $Pr_m = 1$ , used in the main body of this paper, we adopt  $C_\gamma \approx 0.5$  and  $C_k \approx 1.05$ .

It is worth noting that for  $S_a < 10^4$ , the measured growth rates begin to deviate from the expected asymptotic scaling. This regime includes the Lundquist numbers accessible in our nonlinear numerical simulations, and therefore direct comparison to theory is limited by this departure. Nonetheless, the eigenvalue analysis confirms the validity of the scaling laws in the asymptotic regime, and provides consistent estimates of the proportionality constants used in our analysis.

## B. LONG-TERM SIMULATION

In this appendix, we show, in Fig. 12, the colormaps of the current density magnitude ( $|\mathbf{J}| = |\nabla \times \mathbf{B}|$ ) of our long-term 2D MHD simulation for  $S = 10^5$  and  $h = 1/16384$ , at different snapshots. We notice that plasmoids are formed in the high-Lundquist number regime, but are advected out of the domain, even in runs lasting up to  $t_{\max} = 10 t_A$ .

## REFERENCES

Alvelius, K. 1999, Physics of Fluids, 11, 1880

Beg, R., Russell, A. J., & Hornig, G. 2022, The Astrophysical Journal, 940, 94

Beresnyak, A. 2016, The Astrophysical Journal, 834, 47, doi: [10.3847/1538-4357/834/1/47](https://doi.org/10.3847/1538-4357/834/1/47)

Berlok, T., & Pfrommer, C. 2019, Monthly Notices of the Royal Astronomical Society, 485, 908, doi: [10.1093/mnras/stz379](https://doi.org/10.1093/mnras/stz379)

Bhattacharjee, A., Huang, Y.-M., Yang, H., & Rogers, B. 2009, Physics of Plasmas, 16, 112102

Birk, G. T., & Otto, A. 1991, Physics of Fluids B, 3, 1746, doi: [10.1063/1.859693](https://doi.org/10.1063/1.859693)

Birn, J., & Hesse, M. 2001, J. Geophys. Res., 106, 3737, doi: [10.1029/1999JA001001](https://doi.org/10.1029/1999JA001001)

Biskamp, D. 1986, The Physics of fluids, 29, 1520

Büchner, J. 2006, SSRv, 124, 345, doi: [10.1007/s11214-006-9094-x](https://doi.org/10.1007/s11214-006-9094-x)

Cerutti, B., Uzdensky, D. A., & Begelman, M. C. 2012, The Astrophysical Journal, 746, 148, doi: [10.1088/0004-637X/746/2/148](https://doi.org/10.1088/0004-637X/746/2/148)

Chiou, S. W., & Hau, L. N. 2002, Geophys. Res. Lett., 29, 1815, doi: [10.1029/2002GL014720](https://doi.org/10.1029/2002GL014720)

—. 2003, Physics of Plasmas, 10, 3813, doi: [10.1063/1.1606682](https://doi.org/10.1063/1.1606682)

Comisso, L., Grasso, D., & Waelbroeck, F. L. 2015, Physics of Plasmas, 22, 042109, doi: [10.1063/1.4918331](https://doi.org/10.1063/1.4918331)

Coppi, B., Galvao, R., Pellat, R., Rosenbluth, M., & Rutherford, P. 1976, Soviet Journal of Plasma Physics, 2, 533

Daughton, W., Roytershteyn, V., Albright, B. J., et al. 2009, Phys. Rev. Lett., 103, 065004, doi: [10.1103/PhysRevLett.103.065004](https://doi.org/10.1103/PhysRevLett.103.065004)

de Gouveia Dal Pino, E. M., Kowal, G., Kadowaki, L. H. S., Piovezan, P., & Lazarian, A. 2010b, International Journal of Modern Physics D, 19, 729, doi: [10.1142/S0218271810016920](https://doi.org/10.1142/S0218271810016920)

de Gouveia Dal Pino, E. M., & Lazarian, A. 2005, A&A, 441, 845, doi: [10.1051/0004-6361:20042590](https://doi.org/10.1051/0004-6361:20042590)

de Gouveia Dal Pino, E. M., & Medina-Torrejon, T. E. 2024, arXiv e-prints, arXiv:2410.13071, doi: [10.48550/arXiv.2410.13071](https://doi.org/10.48550/arXiv.2410.13071)

de Gouveia Dal Pino, E. M., Piovezan, P. P., & Kadowaki, L. H. S. 2010a, A&A, 518, A5, doi: [10.1051/0004-6361/200913462](https://doi.org/10.1051/0004-6361/200913462)

Ferreira-Santos, G. L., Kowal, G., & Falceta-Gonçalves, D. A. 2025, arXiv e-prints, arXiv:2503.12702, doi: [10.48550/arXiv.2503.12702](https://doi.org/10.48550/arXiv.2503.12702)

Furth, H. P., Killeen, J., & Rosenbluth, M. N. 1963, The Physics of Fluids, 6, 459, doi: [10.1063/1.1706761](https://doi.org/10.1063/1.1706761)

Giannios, D. 2010, Monthly Notices of the Royal Astronomical Society: Letters, 408, L46, doi: [10.1111/j.1745-3933.2010.00925.x](https://doi.org/10.1111/j.1745-3933.2010.00925.x)

Giannios, D., Uzdensky, D. A., & Begelman, M. C. 2009, MNRAS, 395, L29, doi: [10.1111/j.1745-3933.2009.00635.x](https://doi.org/10.1111/j.1745-3933.2009.00635.x)

Goldsmith, D. W. 1970, ApJ, 161, 41, doi: [10.1086/150511](https://doi.org/10.1086/150511)

Heyvaerts, J., & Priest, E. 1984, Astronomy and Astrophysics, 137, 63

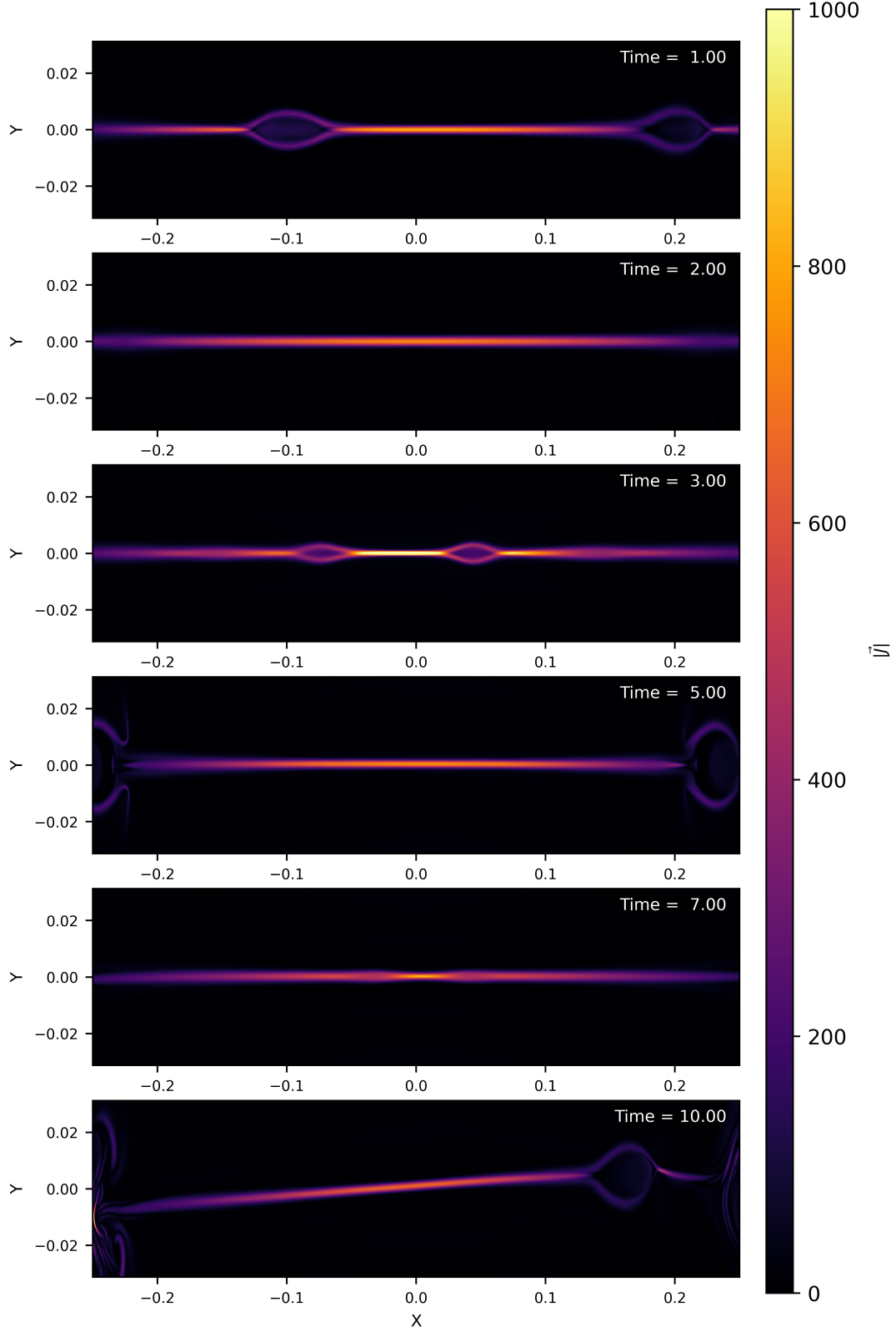


**Figure 12.** Colormaps of the current density magnitude  $|\mathbf{J}| = |\nabla \times \mathbf{B}|$  at different times for the simulation with  $S = 10^5$  and  $h = 1/16384$ . We zoomed in the region  $(x, y) \in [-0.25, 0.25] \times [-0.025, 0.025]$ .

Hosseinpour, M., Bian, N., & Vekstein, G. 2009, Physics of Plasmas, 16, 012104, doi: [10.1063/1.3068470](https://doi.org/10.1063/1.3068470)

Huang, Y.-M., & Bhattacharjee, A. 2010, Physics of Plasmas, 17. <https://doi.org/10.1063/1.3420208>

—. 2016, The Astrophysical Journal, 818, 20, doi: [10.3847/0004-637X/818/1/20](https://doi.org/10.3847/0004-637X/818/1/20)

Huang, Y.-M., Bhattacharjee, A., & Forbes, T. G. 2013, Physics of Plasmas, 20, 082131, doi: [10.1063/1.4819715](https://doi.org/10.1063/1.4819715)

Huang, Y.-M., Comisso, L., & Bhattacharjee, A. 2017, The Astrophysical Journal, 849, 75, doi: [10.3847/1538-4357/aa906d](https://doi.org/10.3847/1538-4357/aa906d)

Jara-Almonte, J., Ji, H., Yamada, M., Yoo, J., & Fox, W. 2016, Phys. Rev. Lett., 117, 095001, doi: [10.1103/PhysRevLett.117.095001](https://doi.org/10.1103/PhysRevLett.117.095001)

Kadowaki, L. H. S., de Gouveia Dal Pino, E. M., Medina-Torrejón, T. E., Mizuno, Y., & Kushwaha, P. 2021, The Astrophysical Journal, 912, 109, doi: [10.3847/1538-4357/abee7a](https://doi.org/10.3847/1538-4357/abee7a)

Kadowaki, L. H. S., Pino, E. M. d. G. D., & Singh, C. B. 2015, The Astrophysical Journal, 802, 113, doi: [10.1088/0004-637X/802/2/113](https://doi.org/10.1088/0004-637X/802/2/113)

Khiali, B., de Gouveia Dal Pino, E. M., & del Valle, M. V. 2015, Monthly Notices of the Royal Astronomical Society, 449, 34, doi: [10.1093/mnras/stv248](https://doi.org/10.1093/mnras/stv248)

Kivelson, M. G., & Russell, C. T. 1995, Introduction to space physics (Cambridge university press)

Kowal, G., Falceta-Gonçalves, D. A., Lazarian, A., & Vishniac, E. T. 2017, ApJ, 838, 91, doi: [10.3847/1538-4357/aa6001](https://doi.org/10.3847/1538-4357/aa6001)

Kowal, G., Lazarian, A., Vishniac, E. T., & Otmianowska-Mazur, K. 2009, ApJ, 700, 63, doi: [10.1088/0004-637X/700/1/63](https://doi.org/10.1088/0004-637X/700/1/63)

—. 2012, Nonlinear Processes in Geophysics, 19, 297, doi: [10.5194/npg-19-297-2012](https://doi.org/10.5194/npg-19-297-2012)

Kulpa-Dybel, K., Kowal, G., Otmianowska-Mazur, K., Lazarian, A., & Vishniac, E. 2010, A&A, 514, A26, doi: [10.1051/0004-6361/200913218](https://doi.org/10.1051/0004-6361/200913218)

Lazarian, A., Eyink, G. L., Jafari, A., et al. 2020, Physics of Plasmas, 27, 012305, doi: [10.1063/1.5110603](https://doi.org/10.1063/1.5110603)

Lazarian, A., & Vishniac, E. T. 1999, The Astrophysical Journal, 517, 700

Lee, L., & Fu, Z. 1985, Geophysical Research Letters, 12, 105

—. 1986, Journal of Geophysical Research: Space Physics, 91, 6807

Lipps, F. B. 1963, Journal of the Atmospheric Sciences, 20, 120, doi: [10.1175/1520-0469\(1963\)020\(0120:SOJIAD\)2.0.CO;2](https://doi.org/10.1175/1520-0469(1963)020(0120:SOJIAD)2.0.CO;2)

Loureiro, N., Schekochihin, A., & Cowley, S. 2007, Physics of Plasmas, 14, 100703

Loureiro, N. F., Samtaney, R., Schekochihin, A. A., & Uzdensky, D. A. 2012, Physics of Plasmas, 19, 042303, doi: [10.1063/1.3703318](https://doi.org/10.1063/1.3703318)

Loureiro, N. F., Uzdensky, D. A., Schekochihin, A. A., Cowley, S. C., & Yousef, T. A. 2009, Monthly Notices of the Royal Astronomical Society: Letters, 399, L146, doi: [10.1111/j.1745-3933.2009.00742.x](https://doi.org/10.1111/j.1745-3933.2009.00742.x)

Masuda, S., Kosugi, T., Hara, H., Tsuneta, S., & Ogawara, Y. 1994, Nature, 371, 495, doi: [10.1038/371495a0](https://doi.org/10.1038/371495a0)

Matthaeus, W., & Lamkin, S. 1985, The Physics of fluids, 28, 303

Medina-Torrejón, T. E., de Gouveia Dal Pino, E. M., Kadowaki, L. H. S., et al. 2021, ApJ, 908, 193, doi: [10.3847/1538-4357/abd6c2](https://doi.org/10.3847/1538-4357/abd6c2)

Medina-Torrejón, T. E., de Gouveia Dal Pino, E. M., & Kowal, G. 2023, ApJ, 952, 168, doi: [10.3847/1538-4357/acd699](https://doi.org/10.3847/1538-4357/acd699)

Meshcheriakov, D., Maget, P., Lütjens, H., Beyer, P., & Garbet, X. 2012, Physics of Plasmas, 19, 092509, doi: [10.1063/1.4754000](https://doi.org/10.1063/1.4754000)

Mignone, A. 2007, Journal of Computational Physics, 225, 1427, doi: [10.1016/j.jcp.2007.01.033](https://doi.org/10.1016/j.jcp.2007.01.033)

Mirnov, V. V., Hegna, C. C., & Prager, S. C. 2004, Physics of Plasmas, 11, 4468, doi: [10.1063/1.1773778](https://doi.org/10.1063/1.1773778)

Morillo, J. M. G., & Alexakis, A. 2025, Journal of Fluid Mechanics, 1007, R3, doi: [10.1017/jfm.2025.109](https://doi.org/10.1017/jfm.2025.109)

Nalewajko, K., Giannios, D., Begelman, M. C., Uzdensky, D. A., & Sikora, M. 2011, MNRAS, 413, 333, doi: [10.1111/j.1365-2966.2010.18140.x](https://doi.org/10.1111/j.1365-2966.2010.18140.x)

Nishikawa, K., Dutan, I., Köhn, C., & Mizuno, Y. 2021, Living Reviews in Computational Astrophysics, 7, 1, doi: [10.1007/s41115-021-00012-0](https://doi.org/10.1007/s41115-021-00012-0)

Orszag, S. A., & Tang, C. M. 1979, Journal of Fluid Mechanics, 90, 129, doi: [10.1017/S002211207900210X](https://doi.org/10.1017/S002211207900210X)

Otto, A. 1991, Physics of Fluids B, 3, 1739, doi: [10.1063/1.859692](https://doi.org/10.1063/1.859692)

Parker, E. N. 1957, J. Geophys. Res., 62, 509, doi: [10.1029/JZ062i004p00509](https://doi.org/10.1029/JZ062i004p00509)

Parker, E. N. 1988, Astrophysical Journal, 330, 474

Petschek, H. 1964, in Proc. of AAS-NASA Symp., Vol. 425, NASA Spec. Pub.

Porcelli, F. 1987, Physics of Fluids, 30, 1734, doi: [10.1063/1.866240](https://doi.org/10.1063/1.866240)

Priest, E. R., & Forbes, T. G. 2002, A&A Rv, 10, 313, doi: [10.1007/s001590100013](https://doi.org/10.1007/s001590100013)

Ranocha, H., Dalcin, L., Parsani, M., & Ketcheson, D. I. 2022, Communications on Applied Mathematics and Computation, 4, 2661, doi: [10.1007/s42967-021-00159-w](https://doi.org/10.1007/s42967-021-00159-w)

Samtaney, R., Loureiro, N. F., Uzdensky, D. A., Schekochihin, A. A., & Cowley, S. C. 2009, Phys. Rev. Lett., 103, 105004, doi: [10.1103/PhysRevLett.103.105004](https://doi.org/10.1103/PhysRevLett.103.105004)

Shay, M. A., Drake, J. F., Rogers, B. N., & Denton, R. E. 1999, Geophys. Res. Lett., 26, 2163, doi: [10.1029/1999GL900481](https://doi.org/10.1029/1999GL900481)

Shi, C., Velli, M., Pucci, F., Tenerani, A., & Innocenti, M. E. 2020, ApJ, 902, 142, doi: [10.3847/1538-4357/abb6fa](https://doi.org/10.3847/1538-4357/abb6fa)

Suresh, A., & Huynh, H. T. 1997, Journal of Computational Physics, 136, 83, doi: [10.1006/jcph.1997.5745](https://doi.org/10.1006/jcph.1997.5745)

Sweet, P. A. 1958, in Electromagnetic Phenomena in Cosmical Physics, ed. B. Lehnert, Vol. 6, 123

Syrovatskii, S. I. 1981, ARA&A, 19, 163, doi: [10.1146/annurev.aa.19.090181.001115](https://doi.org/10.1146/annurev.aa.19.090181.001115)

Taylor, J. B. 1986, Rev. Mod. Phys., 58, 741, doi: [10.1103/RevModPhys.58.741](https://doi.org/10.1103/RevModPhys.58.741)

Tenerani, A., Rappazzo, A. F., Velli, M., & Pucci, F. 2015, ApJ, 801, 145, doi: [10.1088/0004-637X/801/2/145](https://doi.org/10.1088/0004-637X/801/2/145)

Ugai, M. 1992, Physics of Fluids B, 4, 2953, doi: [10.1063/1.860458](https://doi.org/10.1063/1.860458)

Uzdensky, D., & Kulsrud, R. 2000, Physics of Plasmas, 7, 4018

Uzdensky, D. A., Loureiro, N. F., & Schekochihin, A. A. 2010, Phys. Rev. Lett., 105, 235002, doi: [10.1103/PhysRevLett.105.235002](https://doi.org/10.1103/PhysRevLett.105.235002)

Vicentin, G. H., Kowal, G., de Gouveia Dal Pino, E. M., & Lazarian, A. 2025, The Astrophysical Journal, 987, 213, doi: [10.3847/1538-4357/addc62](https://doi.org/10.3847/1538-4357/addc62)

Yamada, M., Kulsrud, R., & Ji, H. 2010, Reviews of Modern Physics, 82, 603, doi: [10.1103/RevModPhys.82.603](https://doi.org/10.1103/RevModPhys.82.603)

Yamada, M., Levinton, F. M., Pomphrey, N., et al. 1994, Physics of Plasmas, 1, 3269, doi: [10.1063/1.870479](https://doi.org/10.1063/1.870479)

Yamada, M., Ji, H., Hsu, S., et al. 1997, Physics of Plasmas, 4, 1936, doi: [10.1063/1.872336](https://doi.org/10.1063/1.872336)

Zhang, B., & Yan, H. 2011, ApJ, 726, 90, doi: [10.1088/0004-637X/726/2/90](https://doi.org/10.1088/0004-637X/726/2/90)